# An investigation of the diversity of outcomes along with machine learning in the prediction of ischemia using PET cardiac perfusion imaging

Naipunya Guruprasad

UNIVERSITY OF TURKU

Master's thesis

University of Turku, Turku PET Centre

Faculty of Medicine, Institute of Biomedicine

06.05.2024

Master´s degree in Biomedical Imaging

Research field: PET imaging and image analysis using machine learning.

Credits: 40 ECTS

Supervisors:

1. Dr. Jarmo Teuho

Adjunct Professor, Turku PET Centre, University of Turku

2. Prof. Riku Klén

Assistant Professor (Imaging instrumentation and detection technologies), Turku PET Centre, University of Turku

*Abstract*

University of Turku, Turku PET Centre

Faculty of Medicine, Institute of Biomedicine

Naipunya Guruprasad: “An investigation of the diversity of outcomes along with machine learning in the prediction of ischemia using PET cardiac perfusion imaging”.

Master’s thesis, 62pp.

Master’s Level

May 2024

---

Positron emission tomography (PET) is an advanced, non-invasive medical imaging technology that allows for precise internal imaging. The recent progress in PET technology, particularly in cardiovascular applications, has significantly improved our knowledge of heart-related conditions. PET scans offer clear visuals of blood circulation and cardiac functions, playing an important role in detecting various conditions. One such condition is ischemia, a state where a part of the body lacks sufficient blood and oxygen supply, posing serious risks. This can be fatal and hence the detection of this is incredibly essential. For accurate predictions of such conditions, healthcare professionals rely on specialised software dedicated to segmentation and visualization of PET cardiac perfusion images, and one such software is Carimas. The integration of predictive machine learning models with Carimas not only enhances but also confirms the accuracy of diagnostic findings, revolutionizing the way we approach cardiac care.

The objective was to have individuals from medical and non-medical backgrounds perform segmentation/analysis on Carimas and to then compare them with one another. Additionally, a pre-trained machine learning model uses the data created on the software to predict whether the patient is ischemic or not. This strategy offers a thorough insight of how segmentation techniques used by people with various backgrounds affect the prediction of ischemia, as well as machine learning models.

55 PET cardiac stress perfusion images from ischemic and non-ischemic patients have been used to create polar maps with radiowater [$^{15}O$-$H_2O$] labelling. The Myocardial Blood Flow (MBF) data is compared using statistical tests like the Wilcoxon test, Jaccard Index and Dice Coefficient. The pre-trained The Convolutional Neural Network (CNN) model undergoes K-fold validation to verify its performance.

Our study aimed to evaluate the accuracy of ischemia prediction derived from manual segmentation performed by individuals with diverse backgrounds indeed gives different MBF data which in turn affects the classification of patients. The CNN model, on the other hand, shows a high area under the characteristic curve value indicating good performance that is independent of the level of expertise of the individuals who created the polar maps.

---

**Keywords:** Ischemia, PET Imaging, Carimas, Convolutional neural networks.

**Table of Contents**

## List of abbreviations

| Abbreviation | Meaning |
|---|---|
| **ACC** | Accuracy |
| **AI** | Artificial Intelligence |
| **API** | Application Programming Interface |
| **AUC** | Area Under the Characteristic Curve |
| **Carimas** | CARdiac IMage Analysis System |
| **CAD** | Coronary artery disease |
| **CCTA** | Coronary Computed Tomography Angiography |
| **CNN** | Convolutional Neural Network |
| **CTA** | CT Coronary Angiography |
| **CT** | Computed Tomography |
| **CVD** | Cardiovascular diseases |
| **DICOM** | Digital Imaging and Communications in Medicine |
| **DL** | Deep Learning |
| **FFR** | Fractional flow reserve |
| **F1S** | F1 Score |
| **LAD** | Left anterior descending artery |
| **LADwa** | Left Anterior Descending artery with anomaly |
| **LCx** | Left circumflex artery |
| **MACEs** | Major adverse cardiac events |
| **MBF** | Myocardial blood flow |
| **MFR** | Myocardial flow reserve |
| **ML** | Machine Learning |
| **MPA** | Mimetic pattern-based algorithm |
| **MPI** | Myocardial perfusion Imaging |
| **PACS** | Picture Archive and Communications System |
| **PET** | Positron emission tomography |
| **PRE** | Precision |
| **PTF** | Perfusion Tissue Fraction |
| **RCA** | Right coronary artery |
| **ROC** | Receiver operating characteristic curve |

| | |
|---|---|
| **ROI** | Region of Interest |
| **SEN** | Sensitivity |
| **SPE** | Specificity |
| **SPECT** | Single-photon emission computed tomography |
| **TAC** | Time activity curve |
| **VA** | Vascularization Area |
| **VOI** | Volume of interest |
| **2D-OSEM** | Two-dimensional ordered expectation-maximization algorithm |

# 1 LITERATURE OVERVIEW

## *1.3 Introduction*

Today's healthcare heavily relies on imaging, which offers a detailed and quantifiable insight into the human body's physiology and various health conditions. The field has seen advancements thanks to cutting-edge technologies that are now able to handle large volumes of data, leading to a revolution in healthcare research. Among these advancements, Positron Emission Tomography (PET) imaging has emerged as a radical nuclear imaging technique that provides us with a look into the body's biochemical processes in great detail which helps us in the visualization and quantification of various conditions [4][5].

The effectiveness of PET scans is due to positron annihilation. Positron is a tiny particle that is similar to an electron but with a positive charge. When this particle is released, it interacts with an electron within the body and by annihilation into two gamma rays provides us with useful information. This interaction is critical for generating images that aid in the diagnosis of numerous health conditions, including various types of heart disease [5].

Cardiovascular disease (CVD) continues to be a major concern and is the primary cause of mortality on a worldwide scale. In conditions like ischemia, where there's no adequate blood flow and oxygen delivery to the heart, present a serious risk and a common factor in these CVDs. Unfortunately, the diagnosis of similar conditions have been challenging over the previous decade [6][7][17]. Even though procedures like coronary angiography exist for diagnosing heart issues, there are times when they do not detect any significant blockages, which means the real problem could be something less obvious, like coronary microvascular dysfunction which is a difficult thing to catch and is frequently linked to cardiac-related chest discomfort. [20][21][22][23][24]. That's where imaging, and particularly PET imaging comes in as they are necessary for precision diagnosis. For accurate predictions of such conditions, healthcare professionals rely on specialised software dedicated to segmentation and visualization of PET images, and one such software is Carimas.

Carimas is software specifically built to analyse PET images. It enables doctors to easily examine blood flow patterns and other crucial parameters to detect health issues [14]. The integration of predictive machine learning models with Carimas not only enhances but also confirms the

accuracy of diagnostic findings, revolutionizing the way we approach cardiac care. [1][2][3][10][11][25][26][27].

In this era of Artificial intelligence (AI), Machine learning (ML) is making significant strides in this field too, particularly with approaches like convolutional neural networks (CNNs). These advanced tools are trained to analyse images and have the potential to provide consistent results compared to human analysis as they don't get tired or biased. Despite this, CNNs have not yet been widely used for real-life medical image analysis due to practical challenges such as insufficient data and expensive computational costs. [12][13][28][33].

Deep learning (DL), a subset of ML, utilises neural network layers to systematically extract intricate information from intricate medical pictures. The growing utilization of AI, ML, and DL in medical imaging may mostly be credited to their remarkable capacity to analyse direct cardiac images. By doing analysis, these technologies have the ability to not only properly identify, but also classify myocardial ischemia, resulting in valuable diagnostic insights. These improvements represent a shift in our understanding and treatment of cardiac problems, with AI playing a crucial role in connecting complicated data with clinical decision making. The future of imaging is tightly linked to the advancing capabilities of AI, which provide the potential for enhanced diagnostic accuracy and better patient care.

As AI advances, its potential to change cardiovascular treatment becomes clearer. It is currently being used in several promising applications, such as identifying obstructive coronary artery disease and predicting other heart function indicators in patients [11]. The use of such technologies has made significant improvements in image classification and analysis using CNNs, which holds well for medical imaging. Although concerns exist, such as ethical issues about accessing patient information, but the advantages of employing machine learning for medical diagnostics are too substantial to overlook [25][26][27][28][33].

Our goal is to combine all of these game-changing elements together to make analysing PET images both accurate and efficient. This could be a significant step toward bettering the accuracy and helping healthcare professionals diagnose heart conditions like ischemia successfully since the process of segmentation is currently done manually.

## *1.2 Thesis structure*

In this thesis, we compare the results of the manual segmentation performed on Carimas by individuals from a medical and non-medical background to determine the impact of their expertise on the prediction of ischemia. Additionally, we use a CNN model to assess if it's performance is affected by the level of expertise of the individuals who created the polar maps.

The structure of this thesis is straightforward and is broken down into seven sections: It begins with an introduction that briefs the reader of our study's key elements, emphasizing their importance and showing how they are all linked to one another. Following that, we move on to the aims and research questions where we highlight the primary objective of this research, the identification of the issue, and the placement of the solution that sets the stage for the further analysis

Once we have established an understanding of these research questions, we transition to the background which gives an in depth explanation of why researching in this field is crucial and elaborates, on the fundamental components of the thesis. This part also discusses the inspiration for our research, ensuring that the readers understand the study's core concepts, important terminologies, and objectives.

Our next section is the materials and methods that describe the methodologies we employed and strategies we used to collect data so we could compare outcomes and evaluate the accuracy of ischemia prediction. After gathering the data, we go on to the results and discussion section, where we systematically analyse, evaluate, and interpret the data in order to draw conclusions.

Finally, we conclude our study by consolidating and reflecting upon our findings, emphasizing the significance of our study and its impact, on the field.

## *1.3 Motivation*

This study on PET image segmentation was driven by a practical problem we encountered when using PET cardiac perfusion images and how different analysts produced varied results. This discrepancy gave rise to questions since these outcomes are crucial in the prediction of myocardial ischemia, where the stakes are exceptionally high because early discovery can drastically alter treatment approaches for a disease that, while severe, is often curable if diagnosed

quickly [4][30][31][32]. Correct segmentation is crucial when planning for a treatment or future steps [35] Motivated by the impact of these contradictions and the growing worldwide prevalence of coronary artery disease (CAD), we wanted to explore this further.

Our goal was to figure out why such differences exist and how they impact the identification of ischemia. The integration of AI with non-invasive imaging modalities, notably in nuclear cardiology and PET myocardial perfusion imaging, has enormous potential to improve diagnostic accuracy [3][12].

This study aims to utilise these findings to investigate methods for enhancing the segmentation process and the machine learning methodology in PET myocardial perfusion imaging. The primary objective is to enhance the precision of diagnosis and aid healthcare practitioners in making informed decisions to improve the management of CAD [9].

## *1.4 Previous studies*

ML is being acknowledged as an increasingly valuable approach for improving the identification and classification of myocardial ischemia in PET imaging. Studies have begun to highlight the potential of ML techniques to improve diagnostic accuracy as well.
The majority of existing approaches rely on region-based segmentation algorithms and incorporate thresholding operations [35]

For instance, in Johansson et al. [34] who studied how different experts segment images. They found out that these experts had different approaches when outlining areas of regions of interest (ROI) in the images that resulted in varying interpretations. This variance underlines the subjective nature of the task and opens up opportunities to investigate more standardized methods.

Dewalle-Vignion et al. [35] designed a straightforward framework to evaluate these subjective interpretations. They compared the manual segmentations of a group of experts against one another using clinical data, aiming to identify the method that best aligns with the manual reference standard. This study intended to spotlight the most reliable methods for delineating the heart's affected regions accurately.

Piri et al. [36] compared segmentation accuracy with computer-generated models and found that a tailored ML model closely matched manual methods, with only a slight 6% deviation. This comparison emphasises the growing competence of AI in replicating the nuanced work traditionally done by human hands.

Similarly, Teuho et al. [3] put their own ML model, a custom CNN, to the test against traditional clinical interpretations. Their CNN model achieved an 83% accuracy rate, nudging close to the 87% accuracy achieved by seasoned clinicians.

These findings highlight the constraints of machine learning and human competence. Although some existing techniques utilise region-based segmentation algorithms and thresholding procedures, there is ongoing advancement in merging the efficiency of machine learning with specialised knowledge, indicating the possibility of incorporating it into clinical diagnostics. This suggests that future improvements in these models may eventually provide assistance or improvement to operations such as manual segmentation.

# 2 AIMS AND RESEARCH QUESTIONS

## *2.1 Aims of the study*

This study was inspired by my experience with PET image segmentation, where I was taught the process of segmentation by two individuals in the field with very different backgrounds. Each had their own unique checkpoints and methods for segmenting the images. Surprisingly, even when working with scans from the same patient, their manual segmentation processes yielded different polar maps, which led to a deeper investigation into the subject.

AIM 1: To examine and compare the analytical results between an individual from a medical background and a non-medical background.
AIM 2: To examine and see how the dissimilarities, if found, result in the prediction of ischemia with radiowater labelling.
Aim 3: To check the accuracy using a pre-trained CNN model independent of individuals with varied levels of experience in the prediction of ischemia.

## *2.2 Research questions*

The results at the end of the segmentation process connected directly to predicting ischemic events. So, we dug into these questions to see how they all fit together. This study aims to breakdown these relationships and make sense of how each component connects to the overall picture of ischemia prediction.

RQ1: How much has the analysed result deviated from the clinically verified ground truth following the methodologies used by individuals from diverse backgrounds?
RQ2: To what extent do these alterations in segmentation techniques impact the accuracy of medical condition prediction?
RQ3: Is there an optimal method to segment or analyse these images if one follows checkpoints given by an expert while performing these operations to reduce the inaccuracy?
RQ4: Is the accuracy of the CNN model independent of this manual process?

# 3 Background

With the increase in CVDs, the importance of disease detection and prediction is also rising. Since many CVDs main root cause is insufficient blood and oxygen i.e., ischemia, the early prediction of this can be vital in saving patients' lives. CVD diagnosis has changed dramatically in recent years because of the incorporation of cutting-edge imaging technology. In order to better understand and provide more accurate diagnosis and analysis of CVD, researchers and physicians are increasingly using PET scans and imaging software like Carimas to visualise such dynamic data.

The use of ML algorithms in the study of CVD has expanded research opportunities. ML models have demonstrated a remarkable and predictive analytical skills after being trained on large datasets generated from PET imaging and other sources. ML systems can predict prospective heart problems by spotting detailed patterns in these datasets. Incorporating ML improves illness prediction accuracy while also allowing healthcare providers to take preventative action before situations worsen.

Despite these developments, there is still a significant area of unexplored research in the field of combined potential of PET imaging and ML in the early prediction of ischemia. A method for ischemia prediction can be created by combining the complex insights obtained from PET scans along with the segmentation software with the prediction power of ML algorithms.

## *3.1 Positron Emission Tomography*

Positrons are the antiparticles of electrons. During β+ decay, the nucleus emits a neutrino and a positron. Because of its substantial mass and positive charge, a positron collides with an electron within its surrounding environment.. The term "positron range" refers to the maximum distance a positron may travel, which depends on its energy level [5].

The abbreviation "PET" in PET imaging is associated with the tracers used, which undergoes decay by producing positrons. The choice of tracer is determined by its intended purpose and the unique characteristics of the imaging technology being used. Each tracer exhibits distinct properties, such as its lifespan, method of synthesis, rate of absorption, and picture sharpness, which are determined by the positron range [58]. PET is an advanced and non-invasive medical

imaging technology that allows for precise internal imaging. It provides a distinct benefit in its capacity to accurately and precisely diagnose ischemia, while also evaluating the extent and severity of the illness. It has the ability to precisely identify cardiac tissue that might benefit from revascularization treatments, hence providing guidance for treatment methods. PET is not as readily available as other imaging methods since it utilises ionizing radiation, necessitating a cyclotron facility for the manufacture of radiotracers [12]. In order to accurately examine PET data, which provides information about the amounts of tracers at certain time points, researchers utilise models to assist in quantifying biological aspects such as metabolic rates, blood volume, and flow dynamics [58].

### 3.1.1 15O-Water as a Tracer

Oxygen-15-labelled water, commonly referred to as 15O-water or [15O]H2O, is currently commonly used as a tracer in PET myocardial perfusion imaging (MPI) to measure Myocardial Blood Flow (MBF). Its unique properties set it apart from other tracers like 13N-ammonia, rubidium-82, and 18F-flurpiridaz, that are easily metabolically trapped in the myocardium. 15O-water is readily diffusible and physiologically inert, which means that it does not interfere with the body's metabolism like other tracers do. This is significant because it gives us a clear and direct measurement of blood flow as 15O-water has an extraction fraction close to one, which means that its absorption into the heart muscle is exactly proportionate to the actual blood flow, which does not hinder metabolic processes in the body. This feature makes it extremely dependable for MBF measurement since the assessment is based on how the tracer flows into and out of the heart's tissues, rather than how much is absorbed [13]. When it comes to using PET imaging to measure blood flow, 15O water is a notable choice for measuring blood flow with PET imaging. As stated by Manabe et al., [60] the tracer's high extraction rate enables its use in doses and at short intervals for stress and rest imaging, while also reducing radiation exposure. Although 15O-water has some benefits, it is not frequently used in settings due to its tendency to provide rather indistinct pictures [4][59].

For practical tracer administration, a dosage of 15O-labeled water, generally ranging between 400 - 500 MBq, is injected using equipment such as Hidex Oy's Radiowater Generator in Finland [24]. MPI using radiowater is extremely effective since its activity uptake is proportional to MBF at all ranges. The MBF is then calculated from PET images using a mathematical model that takes into consideration the blood flow inside the myocardium as well as the factors affecting the PET image. This approach gives a thorough examination of suspected CAD, and in the end it gives us

an accurate diagnostic tool that fits with the highest standards of cardiovascular treatment. MBF values obtained through 15O-water PET imaging can be effectively visualised using polar map images that accurately reflect regional MBF that aids in the diagnosis of suspected CAD [19]. The use of software like Carimas, developed at the Turku PET Centre in Finland, caters and enhances the utility of 15O-water in clinical settings. Carimas, in particular, has demonstrated high reliability, with consistent results across different observers regardless of their experience level, underscoring its repeatability and the reproducibility of its analyses [15].

In this study, we employed [15O]H2O as our tracer agent for PET scans focused on quantitative flow analysis. This approach is favoured because it has been shown to be the best for qualitative image analysis when diagnosing myocardial ischemia, offering a more precise assessment of the condition [37][38].

## *3.2 Myocardial Ischemia*

Myocardial ischemia occurs when there is a demand for oxygen from the heart and the lack of supply results in cardiac dysfunction, arrhythmias, myocardial infarctions, and sudden death as shown in figure 1. PET MPI is a diagnostic technique employed to evaluate the blood circulation to the heart muscle under both stress and rest situations. The images produced through this method can be analysed by experts. Potentially processed using advanced learning algorithms for detecting cardiac ischemia. [4]

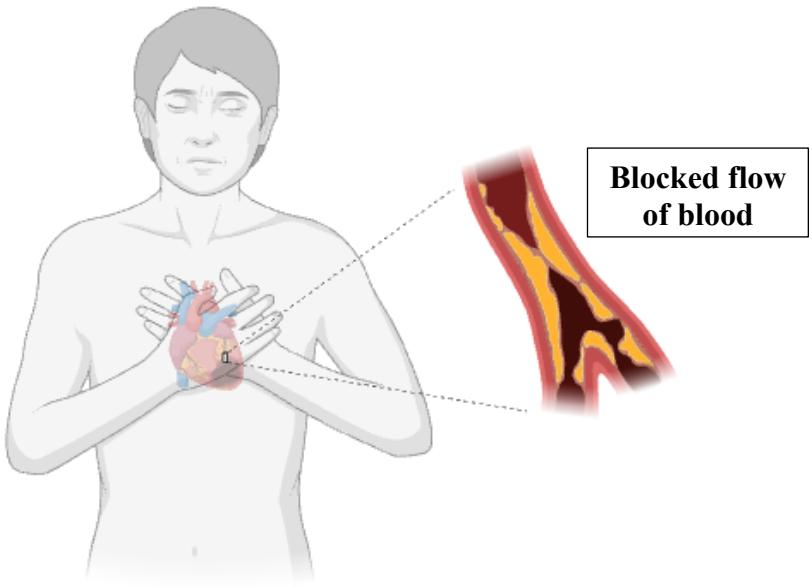


Figure 1. Showing blocked blood flow causing cardia-related symptoms.

Ischemia can manifest due to various factors, such as increased stress on the heart muscle, reduced ability of the blood to deliver oxygen, or a combination of both. The main factor that determines the amount of oxygen supplied to the heart muscle is the flow of blood via the coronary arteries as shown in figure 2. However, this circulation might be adversely affected by several reasons, such as vasospasm, atherosclerosis, or thromboembolic events. On the other hand, the assessment of myocardial oxygen demand relies on several parameters such as contractility, heart rate, and wall stress. Ischemia arises when the oxygen demand of the myocardium exceeds the available supply [62] [63].

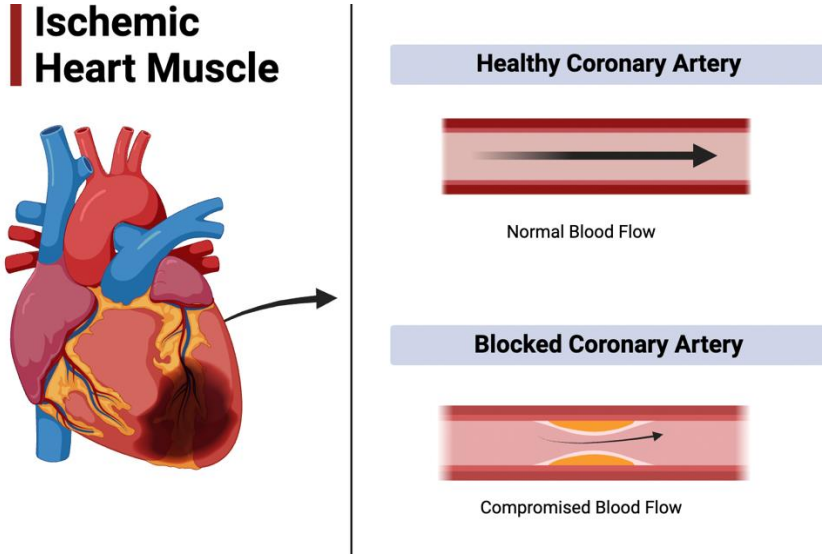


Figure 2. Comparison between sufficient blood flow and insufficient blood flow.

During an ischemic period, myocardial cells undergo hypoxia, leading to impaired aerobic metabolism. As a result, decrease in the pace of energy generation and the accumulation of hydrogen ions and lactate occur. The change in metabolic activities leads to a decrease in the pH value inside the cell, which impairs its functioning and triggers a chain of harmful effects on the heart [64]. Hydrogen ions and lactate in ischemic myocardium can trigger several physiological processes, including inhibition of ion transport across the cell membrane, alterations in intracellular calcium regulation, and activation of proteolytic enzymes. Disruption of ion transport across the cell membrane can lead to cellular depolarization and subsequent damage to the membrane. This event indicated above might cause an elevation in the influx of extracellular calcium ions, which can worsen cellular dysfunction and accelerate cellular death [65].

Prolonged ischemia can lead to a progressive decline in the functioning of the heart muscle due to the lack of oxygen and essential nutrients. This can ultimately result in permanent cellular damage and mortality. Ischemia-induced cell death, referred to as necrosis, typically begins in the subendocardial region of the heart. The high oxygen demands and limited collateral blood flow of this area make it especially vulnerable to ischemia injury. If the ischemiac event persists, there is a chance that necrosis may develop, affecting a larger portion of the myocardium and leading to the occurrence of myocardial infarction [66].

## *3.3 Carimas*

PET imaging is an advanced technique used to quantify cardiac activity and patients are administered a chemical that releases positrons. Positrons in the body interact with electrons, resulting in the production of detectable gamma photons by the scanner. The resultant pictures provide a temporal perspective on the cardiac activity, which is crucial for evaluating physiological processes like metabolism and blood circulation that may not be visible in static images. Because of their cylindrical form and intricate geometry, heart images sometimes require certain viewing orientations. Carimas makes this easier by allowing the user to define axes from which the heart may be examined. Once these axis's are established, the system can segment and analyse the heart's structure, compute values automatically, and provide a polar map that aids in the identification of any anomalies or defects in the heart.

Carimas, short for the Cardiac Image Analysis System was developed to assess complex cardiac imaging data. It specialises in the management of three-dimensional and four-dimensional images. It plays a crucial role in generating detailed polar maps of myocardial perfusion. The importance of Carimas lies in its capacity to assist healthcare practitioners in the diagnosis of cardiac problems, monitoring patients' progress over time, and planning for medical procedures or treatments.

The software analyses PET imaging data by taking sequential images of the heart in layers. The heart is represented in three dimensions by combining layers collected from different angles, with time acting as the fourth dimension. In order to efficiently process accurate images, it is vital to use a program such as Carimas. Carimas is specifically developed to provide a user-friendly and efficient experience by assisting users in activities such as uploading images, segmenting them, analysing data, and displaying conclusions.

Users may achieve a thorough understanding of the heart by seeing images from various perspectives and slicing 3D representations, thereby providing flexibility. Carimas is very adaptable due to its API (Application Programming Interface), which allows for seamless integration of functionality via plugins. The ability to adapt allows for customization to align with the objectives of various research tasks, eliminating the need to create a completely new software system. The system is furthermore compatible with the outputs of imaging scanners, namely the Digital Imaging and Communications in Medicine (DICOM) format, and may be seamlessly connected with hospital systems such as Picture Archive and Communications System (PACS) to facilitate convenient access to patient pictures. The current version of Carimas has a central module, CarimasCore, together with three additional plugins that offer specific functionality for managing, visualizing, and analysing data. The HeartPlugin is mostly used for managing PET data, whereas HeartModels provides specialised tools for heart modeling.

Carimas distinguishes itself from other imaging software by offering extensive PET imaging features that allow for the visualization of 4D data and have the potential for future research and therapeutic applications. The tool's exceptional compartmental modeling capabilities are particularly remarkable, as they allow it to effectively manage tracer chemicals and mimic models, a feature that is not typically seen in software that primarily focuses on static MRI and CT pictures. Carimas offers a wide variety of tools that are quite beneficial for persons who are researching the heart and assessing perfusion using PET imaging. Carimas, with its extensive two-decade track record, has shown itself to be an invaluable asset in both research and therapy settings [67].

### 3.3.1 Polar Maps

From the Carimas software, one of the main results we get are the polar maps. A three-dimensional and four-dimensional dynamic PET image contains a lot of data points and its important for us to visualise and analyse this in a 2D polar map format. It uses kinetic modelling techniques to measure the rate at which radiotracers flow from the circulation to tissues. This is done by applying a single-tissue compartment model for radiotracers. However, a two-tissue compartment model is preferred for tracers that undergo metabolism within the cardiac muscle [93].

From the figure 3. we can see the original PET image that is getting segmented and converted into a polar map following the 17 segment model for the left ventricle segmentation.

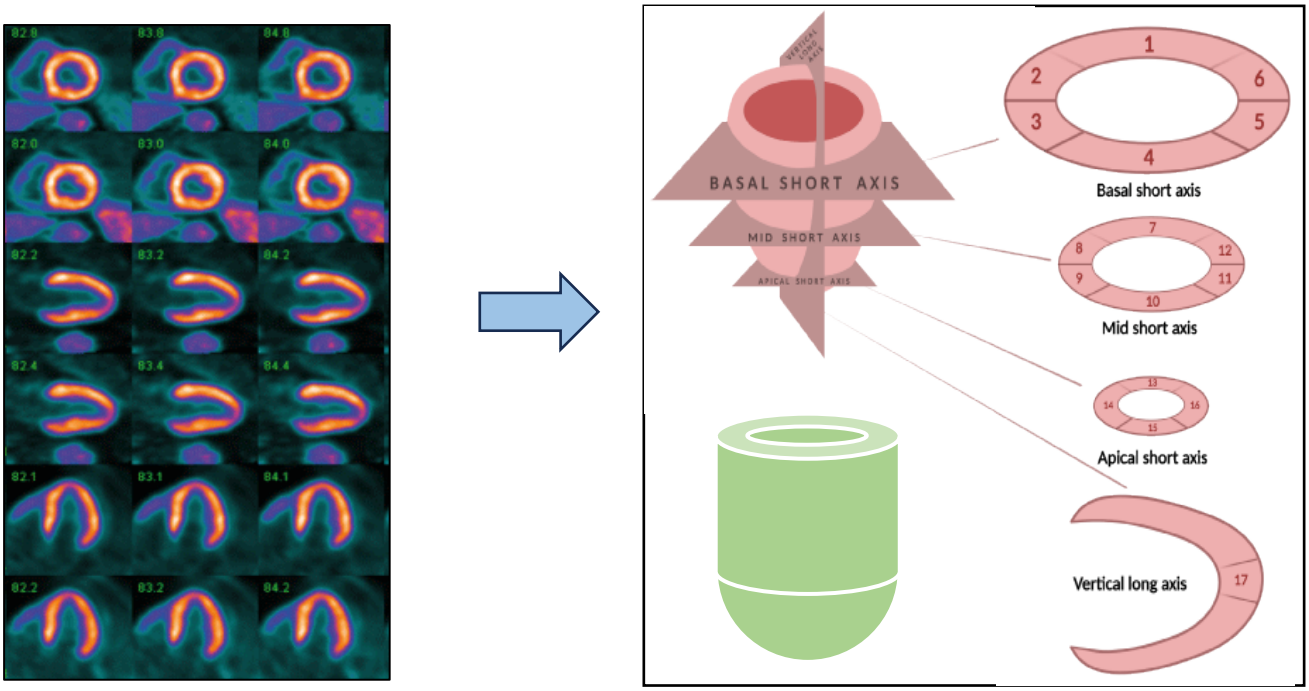


PET-CT scan of normal myocardium

17 segment model for left ventricle segmentation

Figure 3.The process of segmentation and conversion of dynamic PET image into 17 segment polar map [93].

And once we have the 17 segment polar map images, we can visually classify the patient as ischemic and non-ischemic as make the classification as seen in figure 4.

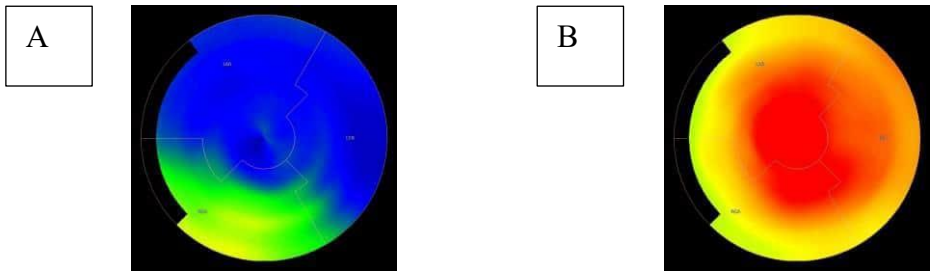


Figure 4. An example of ischemic polar map (A) with more green and colours and non-ischemic polar map (B) with more red and yellow colours.

## *3.4 PET imaging for the diagnosis of myocardial ischemia*

Over the years, imaging techniques such as Single-photon emission computed tomography (SPECT) and PET MPI have become essential tools for addressing ischemic heart diseases. The PET MPI technique is great for its capacity to conduct stress testing and assess MBF in a single examination [1][32][46]. The uses of PET in cardiology mostly involve the measurement of blood flow and the assessment of cardiac metabolism in instances when there is ischemia in the left ventricles. PET scans have yielded insights on the relationship between ischemia and cardiac disorders [2][4] [47][48]. Comparative studies have demonstrated that PET is more precise than Coronary Computed Tomography Angiography (CCTA) and SPECT in diagnosing myocardial ischemia in individuals suspected of CAD, with results corroborated by fractional flow reserve (FFR) measures. Prior to 2017, European specialists did not have a preference for a particular noninvasive imaging approach. However, when directly comparing its capacity to identify ischemia with that of SPECT MPI, quantitative PET has demonstrated higher performance [37].

MPI plays a great role in nuclear medicine by assessing MBF to help diagnose potential CAD. The use of radiowater also known as oxygen-15 labelled water as a tracer in MPI has proven effective since its absorption is closely correlated with blood flow levels, even at elevated rates. This oxygen-based tracer provides a notable benefit in the detection of CAD by allowing for accurate assessment of blood flow in the heart muscle using PET images. The determination of blood flow is an elaborate procedure that takes into account both the flow of blood in the heart and the variables that impact the PET image [12]. The use of 15O water MPI in PET imaging is

highly effective for assessing perfusion by offering accurate measurement of MBF in both rest and stress imaging. Although the technique for quantifying MBF using PET in CAD research is widely recognised, it is crucial to acknowledge the constraints of currently accessible radiotracers. Radioactive water is employed for the measurement of MBF, however its limited half-life limits its usage to facilities equipped with an on-site cyclotron. The short duration of the half-life also affects the quality of the image by creating temporal activity curves, which impede precise measurement of myocardial perfusion. An optimal perfusion compound would possess a high initial extraction fraction and have the ability to accurately measure regional MBF throughout a broad spectrum, thereby allowing for exact calculation of absolute MBF [38].

Disease presence is identified by a specific reduction in regional stress MBF (sMBF) or myocardial flow reserve (MFR), using predetermined threshold values for the tracers employed. PET data gathering and processing, facilitated by software such as Carimas MBF, allows for the visual representation of MBF in several regions of the heart, including the right coronary artery (RCA), left anterior descending (LAD) artery, and left circumflex (LCx) artery. The precision of this method in diagnosing CAD by invasive angiography and FFR measures has made it more popular for examining patients with suspected CAD [37][49]. The assessment of cardiac perfusion data begins with the orientation of the heart, but it is later automated using algorithms that can detect specific parts of the myocardium. Modifications to the ROIs are performed manually as required. Experts from several domains have thoroughly evaluate this procedure to determine its influence on MBF readings and its capacity to predict ischemia [3]. Tissue time activity curves are derived from polar maps by utilizing specific ROIs. A blood pool time activity curve is produced from a tiny ROI positioned at the middle of the left ventricle on the final frame of dynamic short axis pictures. This comprehensive procedure is suitable for analysing both resting and stress data in order to precisely detect CAD. The prospective application of PET imaging to evaluate risk in different clinical circumstances is promising since it combines assessments of relative perfusion with absolute measurements of cardiac blood flow [38].

Identifying ischemia with PET scans is a strong and separate indicator for long-term mortality and cardiovascular events. Research suggests that a reduction in sMBF or MFR might serve as prognostic markers, providing predictive value that goes beyond regional ischemia and other risk factors. The use of [15O]water PET enables the measurement of sMBF, and the interpretations are based only on quantitative data. An sMBF value of 2.3 ml/g/min or less is regarded a reliable sign of obstructive CAD, which is characterized by a FFR below 0.80 at both the patient and vascular levels. However, the process of identifying the specific threshold value for global

sMBF that may accurately predict bad clinical outcomes in patients undergoing examination for suspected CAD using [15O]water PET imaging is still an area that needs more research and analysis. When analysing heart segments, it is typical to exclude some sections, such as segments 2 and 3 in the basal septum and segment 17. A sMBF value of 2.3 ml/g/min or lower in any segment shows decreased blood flow compared to a sMBF value over 2.3 ml/g/min, which is used to assess the health of the heart [52]. The threshold was established in experiments to identify ischemia, which manifests as perfusion deficits in at least two adjacent myocardial segments at these flow circumstances [37].

Furthermore, PET perfusion imaging can be utilised to identify coronary microvascular dysfunction by assessing the vasodilator capacity in patients experiencing stable chest discomfort and suspected (CAD) [24]. Quantitative PET perfusion imaging stands out among diagnostic approaches for heart diseases due to its high diagnostic accuracy when compared to invasive coronary angiography standards, as well as its capacity to anticipate major adverse cardiac events (MACEs) [53][54][55]. Hence, quantitative PET perfusion imaging serves as a means to detect CAD-induced ischemia and evaluate the likelihood of MACEs without the need for invasive procedures [10]. Efficiently managing cardiac diseases, such as myocardial ischemia, requires prioritizing the use of modern imaging techniques like nuclear imaging to promptly identify and address potential significant health problems. PET and other nuclear imaging techniques have gained popularity in the identification of ischemia. Medical practitioners commonly examine PET MPI images, however the utilization of AI-enhanced computer-aided diagnostic techniques can significantly benefit in interpretations. AI may also assist with activities such as image classification in the medical area, which is crucial for illness identification. An example of a classification issue in medical diagnosis is the identification of ischemia using polar map image data. Clinicians must assess whether the map shows a normal or pathological state [1][10][12][56][57].

### *3.5 AI for Cardiovascular disease*

AI has become an essential component of modern healthcare, especially in the studying and treatment of CVDs. Its uses have led to new findings in heart failure and congenital heart diseases, resulting in novel treatments. AI can also assist in monitoring how medications perform once they are released to the market [39]. The investigation of AI's function in CVD is, however, not novel.

In 1963, Warner et al. [40][41] and Gorry and Barnett in 1968 investigated how computer algorithms and mathematical models may assist in identifying congenital heart disease. Warner and his colleagues created a mathematical model based on Bayes' theorem to demonstrate that with the correct data, a computer can equal a doctor's diagnosis accuracy. However, this strategy wasn't ideal; it occasionally missed critical diagnoses and might lead to unneeded testing, especially when employed by someone less skilled. [40][41]. More recently, Zellweger et al. [44][45] investigated AI's potential as a non-invasive technique for detecting CAD. They applied an AI-based mimetic pattern-based algorithm (MPA) and discovered that it beat standard risk scores such as the Framingham risk score in detecting CAD. The MPA had a remarkable positive predictive value, scoring well in both the training and test groups [39][44][45].

Quantitative PET myocardial polar maps are one use of how AI can help in cardiovascular imaging as these maps provide a thorough picture of blood flow in the heart's left ventricle, which is extremely valuable for patients with known or suspected CAD [43]. AI does more than simply diagnose; it enhances cardiovascular care practice by incorporating precision medicine and big data analysis. This allows us to correctly filter through various clinical data for predictions and classifications without making assumptions. This can be a game changer for busy healthcare systems by automating tedious processes and allowing clinicians to focus on what they do best which is caring for patients [39].

Despite these advancements, implementing AI in healthcare comes with its own challenges. We're talking about concerns like data privacy, the use of obsolete or biased data, which can lead to incorrect findings. Despite these obstacles, AI's potential to transform healthcare appears obvious [39].

## *3.6 Image classification and ML models*

AI has revolutionized cardiovascular imaging, leading to a paradigm shift in the diagnosis and treatment of CVDs. This transformation is driven by ML, a multidisciplinary domain that empowers algorithms to acquire knowledge from datasets without the need for explicit programming for specific tasks. An established instance in this domain is the CNN, with several layers of nodes that handle input. CNNs are highly efficient in image processing and data management, thanks to their learning processes. They enhance cardiac image analysis and enable precise classification of myocardial ischemia [39].

ML, as a subset of AI, enables systems to extract valuable information from data and provide accurate predictions. It generates models that detect data patterns by employing diverse mathematical functions, efficiently automating programming with minimum human involvement. Nevertheless, human oversight is crucial, particularly when deciding how to implement machine learning techniques in the field of medicine [77][78]. Deep learning, a subset of ML, utilises neural network layers to systematically extract intricate information from intricate medical pictures. The growing utilization of AI, ML, and DL in medical imaging may mostly be credited to their remarkable capacity to analyse direct cardiac images. By doing analysis, these technologies have the ability to not only properly identify, but also classify myocardial ischemia, resulting in valuable diagnostic insights. These improvements represent a shift in our understanding and treatment of cardiac problems, with AI playing a crucial role in connecting complicated data with clinical decision making. The future of imaging is tightly linked to the advancing capabilities of AI, which provide the potential for enhanced diagnostic accuracy and better patient care. In figure 5, we can see a diagrammatic overview about the hierarchy of AI.

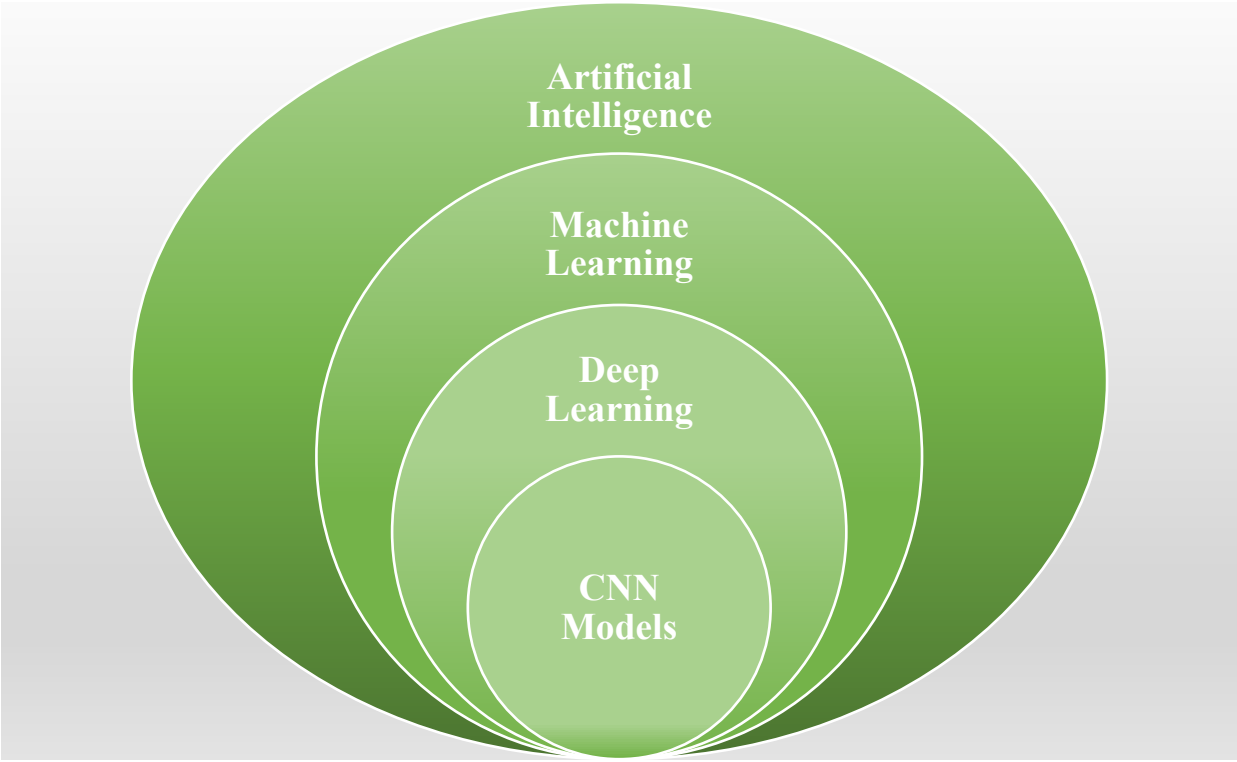


Figure 5. An overview of the world of Artificial intelligence.

DL algorithms, renowned for their capacity to mimic cognitive abilities, have been generating remarkable advancements in the field of medical imaging. The advancement in imaging is

particularly evident in the use of DL for the analysis of brain and cardiac PET/SPECT images. These applications demonstrate the promise of ML for predictive modelling by using image classification to improve diagnostic processes. The capacity to learn and adapt to new situations, together with its effective handling of enormous amounts of data, makes it highly advantageous for classifying medical images [87]. It is especially acknowledged for its capacity to automatically extract features, a procedure that was formerly time-consuming and prone to mistakes. On the other hand, DL algorithms have the ability to autonomously learn and identify certain data characteristics, optimizing them for accurate and dependable medical diagnostics [12]. Thus, DL enhances the accuracy of detecting illnesses and tracking treatment progress. DL techniques encounter difficulties in medical contexts due to the requirement for substantial training datasets, which are sometimes restricted in specialised medical sectors. The requirement for datasets is a significant barrier to the general use of deep learning in domains with limited data accessibility to facilitate efficient model training. In the field of imaging, the task of obtaining sufficient data is particularly challenging due to the scarcity of available information induced by ethical and privacy considerations. Consequently, there is a challenge in acquiring a sufficient amount of labelled data to effectively train these highly capable algorithms since this type of labelled data typically needs to be produced by experts. [90].

CNNs have revolutionized the classification of pictures in the field of imaging. They accomplish this by employing a technique known as convolution, which enables them to not only learn from individual pixels but also understand the surrounding context inside the images. The complex architecture of CNNs consists of convolution layers, pooling layers, and linked layers, as seen in figure 6 which provide an effective foundation for intricate image processing [75][82]. A CNN is one of the neural network architectures commonly employed in DL and they are mostly utilised for tasks such as classification of images as they have demonstrated exceptional achievements in several industries, including medical imaging. Nevertheless, the problem of data scarcity continues to persist when training CNNs for medical image processing, since it requires a significant quantity of data. Transfer learning addresses this issue by utilizing pre-trained CNN models that have been trained on extensive datasets of natural images. These models are then fine-tuned to recognise comparable patterns in medical images [74][75]. Moreover, CNNs extend their capabilities beyond classification of images to the field of predictive modelling. They are characterized by their capacity to exceed constraints in discerning complex patterns inside medical images. Although reliance on training datasets is a problem, CNNs may effectively address novel difficulties in medical imaging by utilizing transfer learning from trained models [79][80][81][92].

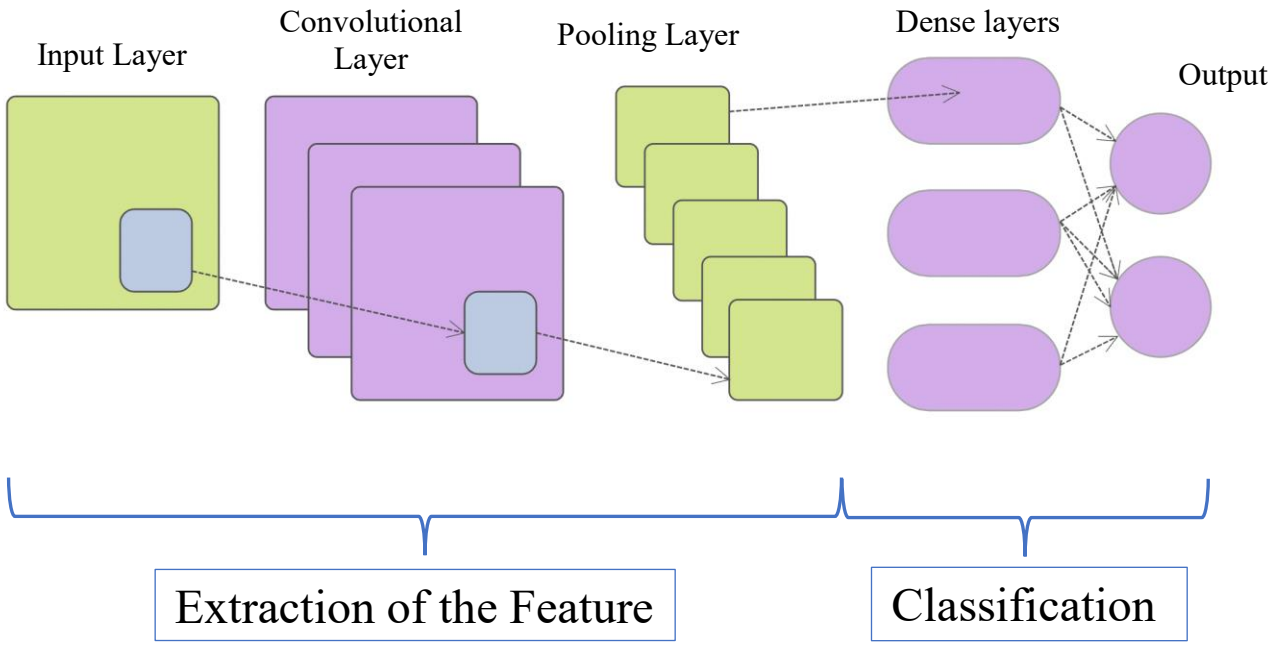


Figure 6. A schematic view of the architecture of a CNN model.

In the field of ML, there is a possibility to identify patients who are at risk of developing myocardial ischemia and are more likely to experience MACE by using accessible predictors and quantitative PET myocardial perfusion imaging. ML is continuously being studied to improve the selection of techniques for cardiovascular diagnosis and prognostic assessments [10]. Although the general use of PET scans is limited due to obstacles related to accessibility, cost, and infrastructure requirements, the integration of data is consistently improving the effectiveness of machine learning. This enhancement might assist in prioritizing the utilization of PET scans for patients who would get the greatest benefit from myocardial perfusion imaging by precisely evaluating the extent and location of ischemia load [10].

AI has greatly enhanced the field of nuclear cardiology, namely in PET MPI. ML has proven to be highly efficient in this field, particularly with the utilization of DL algorithms. DL methods excel in their capacity to extract characteristics from imaging data by employing advanced neural network layers. These algorithms have contributed to improving direct interpretation of cardiac images and diagnosing myocardial ischemia, resulting in improvements in diagnostic accuracy [31][32][43][75][76]. The inherent capacity of learning to autonomously extract characteristics from image data represents a substantial advancement in comparison to conventional approaches of image classification, which are frequently laborious and susceptible to mistakes. DL algorithms are highly effective at identifying important characteristics in data, which is

essential for accurately categorizing and understanding medical images [87]. The main goal of integrating learning in this context is not just to aid in clinical practice but also to foster an impartial viewpoint on myocardial ischemia. In the current healthcare landscape, where clinicians deal with complex diagnostic and prognostic assessments, machine learning models can assist in optimizing these evaluations. The integration of these models with updated electronic patient data has the potential to greatly improve precision medicine and clinical alerts [10][86].

### 3.6.1 Previous studies

Through the integration of clinical and PET data, ML algorithms are being proposed to improve the identification of CAD and guide decisions for early treatment. This development has the capacity to enhance assessments of the risk of death from any cause, using a wide range of clinical indicators obtained by CCTA [84][85][86].

A recent example of this is the study "Classification of ischemia from myocardial polar maps in 15O–H2O cardiac perfusion imaging using a convolutional neural network" authored by Teuho et al. [3]. This study created a specialised CNN model to assess 138 polar maps from 15O–H2O stress perfusion tests. The maps were in JPEG format and categorised individuals as either ischemia or non-ischemic based on the results of invasive coronary angiography, which identified obstructive coronary artery disease. The performance of the model was evaluated using several measures such as accuracy (ACC), the area under the receiver operating characteristic (ROC) curve (AUC), F1 score (F1S), sensitivity (SEN), specificity (SPE), and precision (PRE), highlighting the model's ability to accurately diagnose [4].

Furthermore, the ability of DL to improve diagnosis accuracy has been further proven in a comprehensive SPECT investigation. The study employed 99mTc-sestamibi or 99mTc-tetrofosmin to conduct MPI. It identified polar maps from 1638 participants by comparing them to reference data obtained from invasive coronary angiography. The dataset was enlarged to incorporate data from both semi-upright and supine stress MPI of 1160 individuals who underwent the identical MPI protocol. The results from this comprehensive dataset confirmed that deep learning greatly enhances the automated prediction of obstructive CAD in comparison to current clinical approaches [94].

It is important to mention that although SPECT data has been the main focus of these techniques, just a few publications have explored the use of PET data. Quantitative PET perfusion polar maps

provide a comprehensive dataset for sophisticated analytical approaches, but their full potential has not been fully used. However, there is a significant lack of assessment when it comes to applying ML to a wide range of easily accessible and interrelated predictor variables. These characteristics might significantly help in identifying individuals who are likely to have myocardial ischemia and the related cardiovascular risks, as evaluated using quantitative PET myocardial perfusion. It is expected that advancement in this approach will enable the development of advanced diagnostic skills, leading to better results for patients [3][10].

### 3.6.2 K-Fold cross validation

In our research, we used the features of TensorFlow and Keras, two well-recognised libraries in the field of DL. We evaluated the efficacy of our CNN model by utilizing the AUC, a critical metric in ROC curve analysis that measures the diagnostic accuracy of a classifier system across various discriminating thresholds. An AUC score close to 1 shows precise predictions, whereas an AUC value approaching 0.5 denotes a lack of ability to differentiate [4].

Pretrained models represent a step forward in improving the efficiency of machine learning by utilizing prolonged training on intricate problems with massive datasets and significant computing resources. This extensive training provides these models with a sophisticated understanding of attributes that may be utilised or 'transferred' to. These versatile models may be easily accessed via repositories like as the Keras applications repository and TensorFlow hub. They are frequently evaluated in competitions like ImageNet, where teams compete to create better CNN structures [88][89]. CNNs are carefully crafted to achieve a harmonious equilibrium between efficiency and the inherent strong performance characteristics of ordinary convolutions. CNNs, particularly beneficial in fields like as image and speech recognition, contribute to improving overall performance levels [12].

Within the domain of ML, we explored many learning methods. The one used in our study was the supervised learning algorithms which operates with the use of labelled data, to discover concealed patterns and categorise data according to certain analytical goals. This approach facilitates comprehension of datasets and is particularly useful in situations when there is a scarcity of labelled data or when intricate linkages within the dataset are not completely comprehended [32][75][76].

One often employed method is called k-fold cross-validation. As we can see in figure 7, where the model is trained with k-1 folds and evaluated with the remaining green folds and this is repeated for each blue fold as thus k times. This approach is used to evaluate the ability of a machine learning model to adapt to various datasets, while avoiding the limitations of relying exclusively on a single training and testing split that may not correctly represent the model's real performance. In k-fold cross-validation, the dataset is partitioned into k-equal segments, guaranteeing that each section is utilised for validation precisely once. This thorough technique provides an assessment of the model's performance on several subsets of data. In our research, we utilised 3-fold, 5-fold and 10-fold cross validation to comprehensively assess and compare the difference in the findings.

During the evaluation of ML models in each iteration of k-fold cross validation, performance measures such as accuracy, mean, median and standard deviation are computed. The final assessment of the models is determined by calculating the average of these performance metrics throughout all 'k' iterations. Despite the time and processing resources required, k-fold cross validation is very beneficial due to its ability to decrease biases inherent in data splitting. This technique involves training and evaluating the model 'k' times, resulting in a more accurate and reliable assessment. This technique ensures a reliable and consistent assessment of a model's real performance, which is essential for optimizing hyperparameters, selecting models, and picking features [12].

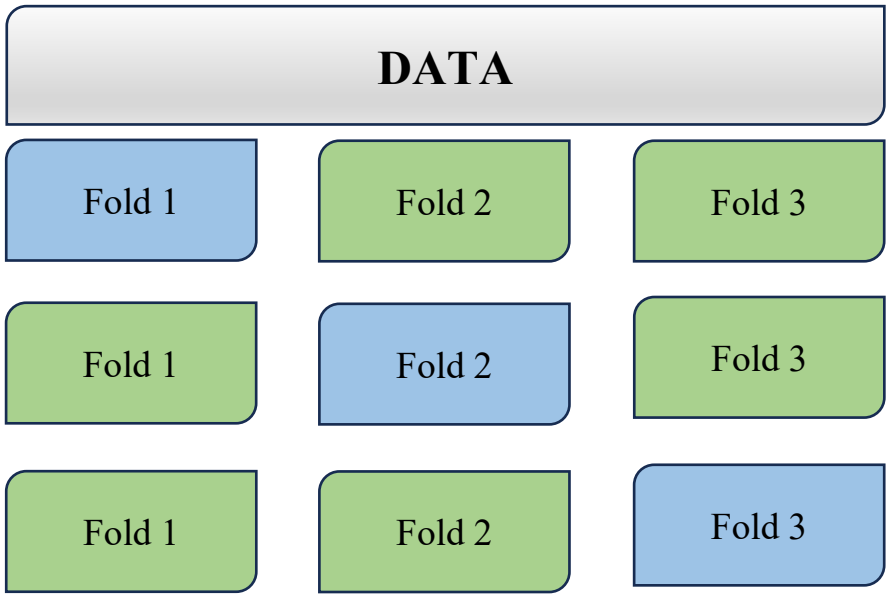


Figure 7. K-fold cross-validation, where k=3

# 4 MATERIALS AND METHODS

## *4.1 Patient population*

In our research, we considered 55 patients that underwent PET imaging with radiowater [$^{15}O$-$H_2O$] labelling. The group comprised of individuals who had a clinically verified history of myocardial infarction, as seen by documented medical evaluations and previous diagnostic procedures (Ischemic) and individuals with non-ischemic cardiac conditions, who had a range of cardiac dysfunctions, excluding those caused by CAD. It was imperative for us to analyse the cardiac images of both groups without any bias. So we made sure not to have any knowledge of which individuals had ischemic conditions and which did not. [3].

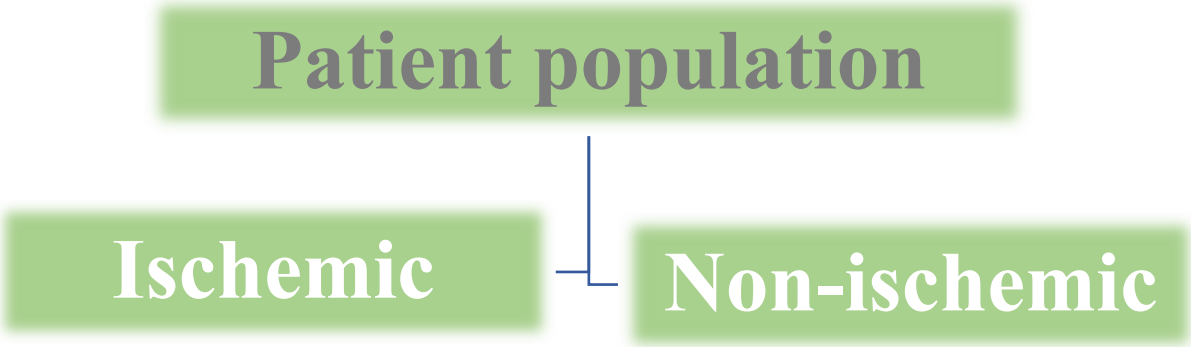


Figure 8. Patient population of the dataset

From these patients, cardiac stress PET cardiac stress perfusion images were obtained. These images depict the flow of blood to our heart muscle, the myocardium, under stressful conditions like physical exercise or using pharmacological drugs to mimic the same effect on the heart. This helps physicians understand how the heart handles the workload to see signs of heart problems.

Based on these images, we conducted a study involving two groups—one with a medical background and the other without. Our objective was to analyse these images on Carimas and see how each group interpreted the images, specifically focusing on their ability to identify and segment details of the heart in the scans that ultimately resulted in the prediction of ischemia.

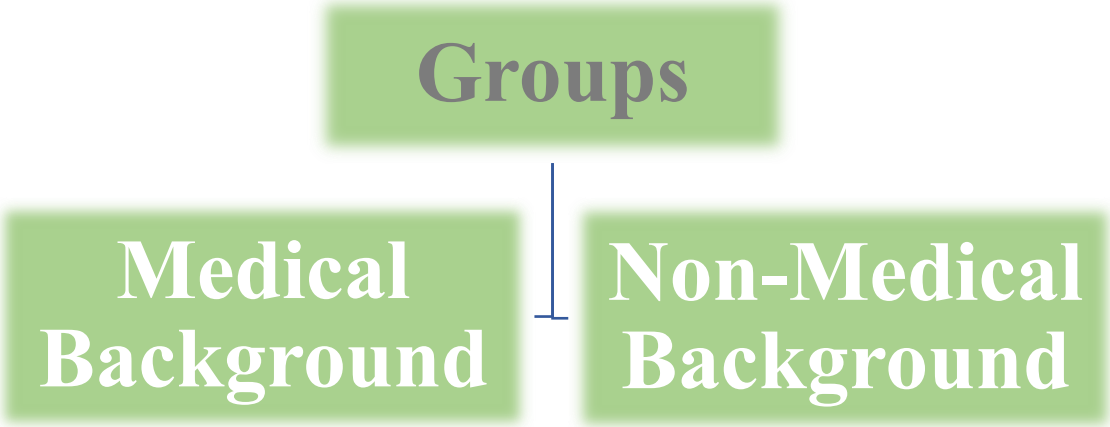


Figure 9. The group of individuals involved in the segmentation process.

In the process of image evaluation, the individual with the medical background who had clinical experience effectively, successfully analysed and segmented all 55 PET images despite some images having noticeable noise. This showcases the importance of medical knowledge in identifying cardiac structures accurately even under challenging image quality.

On the hand, the individual without a medical background approached the task with a different set of skills. Despite being briefly trained for about 2 months in image segmentation and analysis, this individual only found 44 cardiac stress PET images suitable for detailed segmentation. This was mainly to due poor image clarity, high background noise and no clear visualization of the ventricular borders of the heart. Therefore, 11 PET cardiac stress images were not included since they had significant noise that made it difficult to see the specific anatomical characteristics required to accurately spot and segment the left ventricle. These noisy images would also produce unreliable segmentation, making it necessary for their exclusion from the analysis.

This comparative approach highlights the importance of medical experience in assessing cardiac images and provides insight into the difficulties faced by non-specialists when using modern imaging technologies. The findings of this comparative investigation may provide insights into the importance of specialised training and having checkpoints for the segmentation process in understanding complex medical images.


Figure 10. Total patients after the elimination of the noisy cases.

## *4.2 Image Acquisition*

The initial imaging procedure was carried out using a 64-row Discovery VCT PET/CT scanner manufactured by General Electric Medical Systems, USA. The preferred imaging methods were CT coronary angiography (CTA) and MPI using a PET/CT hybrid. A computed tomography (CT) scan was used to adjust for attenuation, followed by a PET scan to assess adenosine-induced stress perfusion. During a time period of two minutes before to the initiation of the scan, a dosage of 140 micrograms of adenosine per kilogram of body weight was injected through the veins. The patient was administered a rapid intravenous infusion of oxygen-15 labeled water (900 to 1100 MBq) using a Radiowater Generator from Hidex Oy, Finland, for a duration of 15 seconds. The heart's blood flow was assessed using a dynamic mode acquisition consisting of several time intervals: 14 intervals of 5 seconds, 3 intervals of 10 seconds, 3 intervals of 20 seconds, and 4 intervals of 30 seconds. The obtained picture data was subsequently rebuilt using a 2D ordered expectation-maximization approach (2D-OSEM) with the specified parameters: a field of view of 35 cm, 2 iterations, a matrix size of 128x128, a Gaussian post-filter with a width of 6.0 mm, and 20 subsets.[12][24]

## *4.3 Data Acquisition*

In this thesis, we used 44 stress PET perfusion images from both the individuals- medical and non-medical background to make it a common ground for an effective comparison. These images were critical in generating the data for further analysis and were segmented to extract key information such as polar maps, data on MBF and Volume of Interest (VOI). The Carimas software platform was the primary tool for image loading and, segmentation.

The images and data were handled using a Lenovo 23-inch FHD ThinkVision T23i-20, which provided the computational power necessary for the intricate processing involved. This high-performance system ensured that the data processing was efficient and reliable, contributing to the integrity of the study's results.

4.3.1 Protocol for segmentation followed by non-medical background individual

The patient file to be analysed was loaded onto Carimas. After the file has been loaded and viewed, we are presented with four quadrants displaying images of the heart as seen in Figure 11.

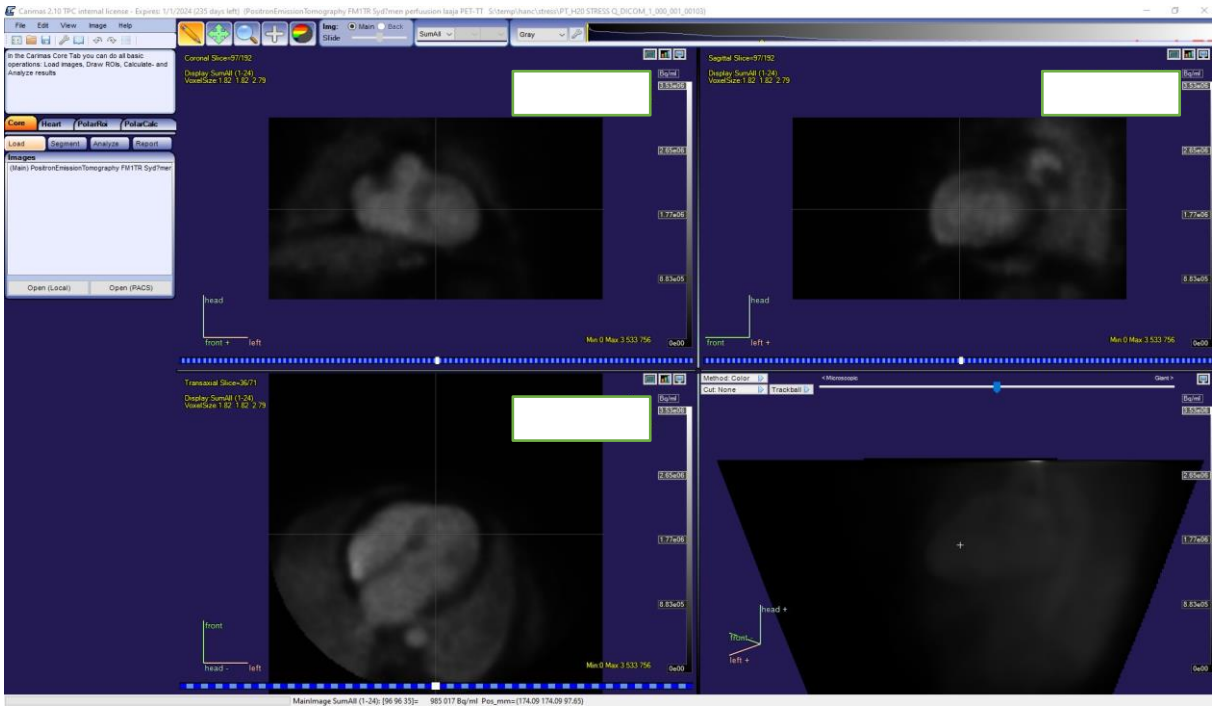

Figure 11. Quadrant images of the heart on Carimas.

By adjusting the contrast, we can effectively visualise the anatomical features of the left and right ventricles. As seen below in Figure 12, it is necessary to label the axis from the base to the apex of the left ventricle in segment A. Moving to segment B, we realign the base and apex axes to the center. In segment C, it is necessary to draw out the axis extending from the center of the right ventricle to the center of the left ventricle, as shown by RV → LV.

The segmentation tools can be found as the second option under the "heart" section of Figure 13, indicated by a grey arrow. By aligning the axis, we have successfully identified and distinguished 14 distinct segments. In this section, we have the chance to adjust the axis in segments A, B, and C of figure 13 by vertically adjusting both the base and apex of the axis to align at the centre. Additionally, we can observe the corresponding changes in current inside these segmented images.

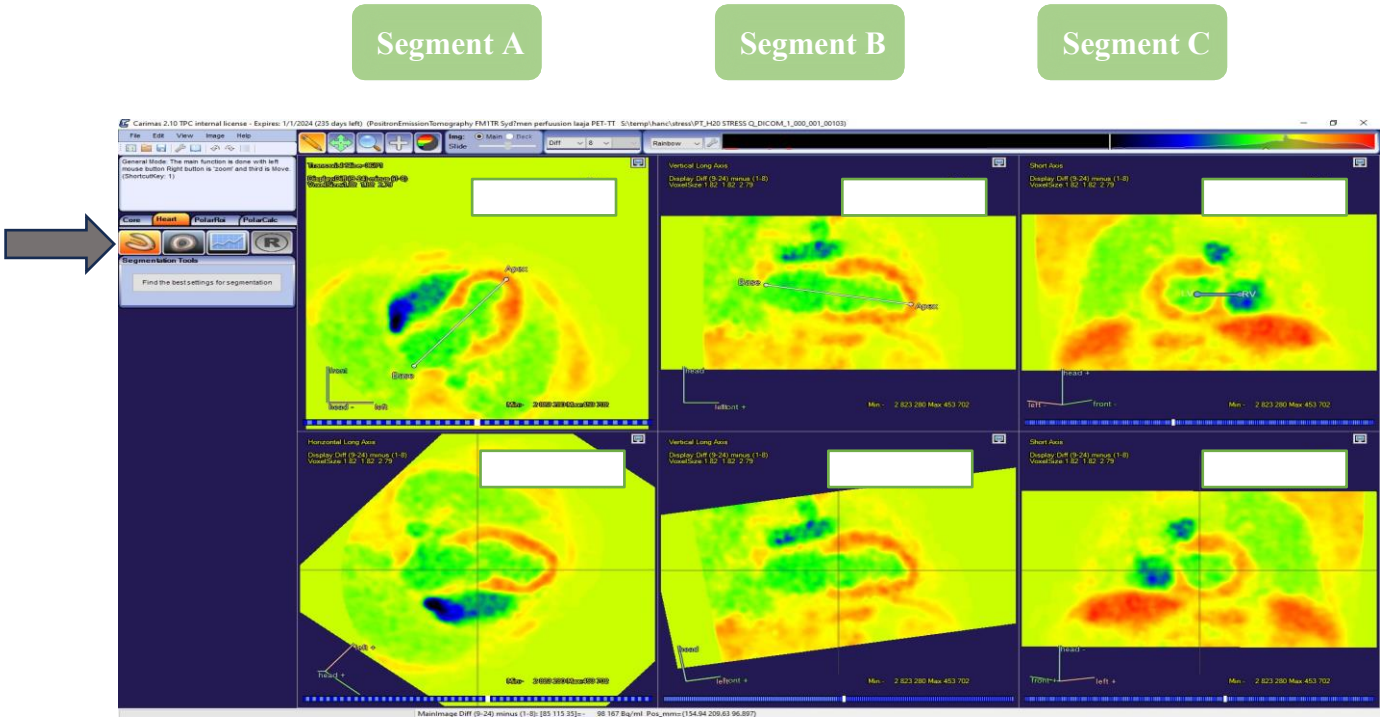


Figure 12. Images undergoing segmentation on Carimas.

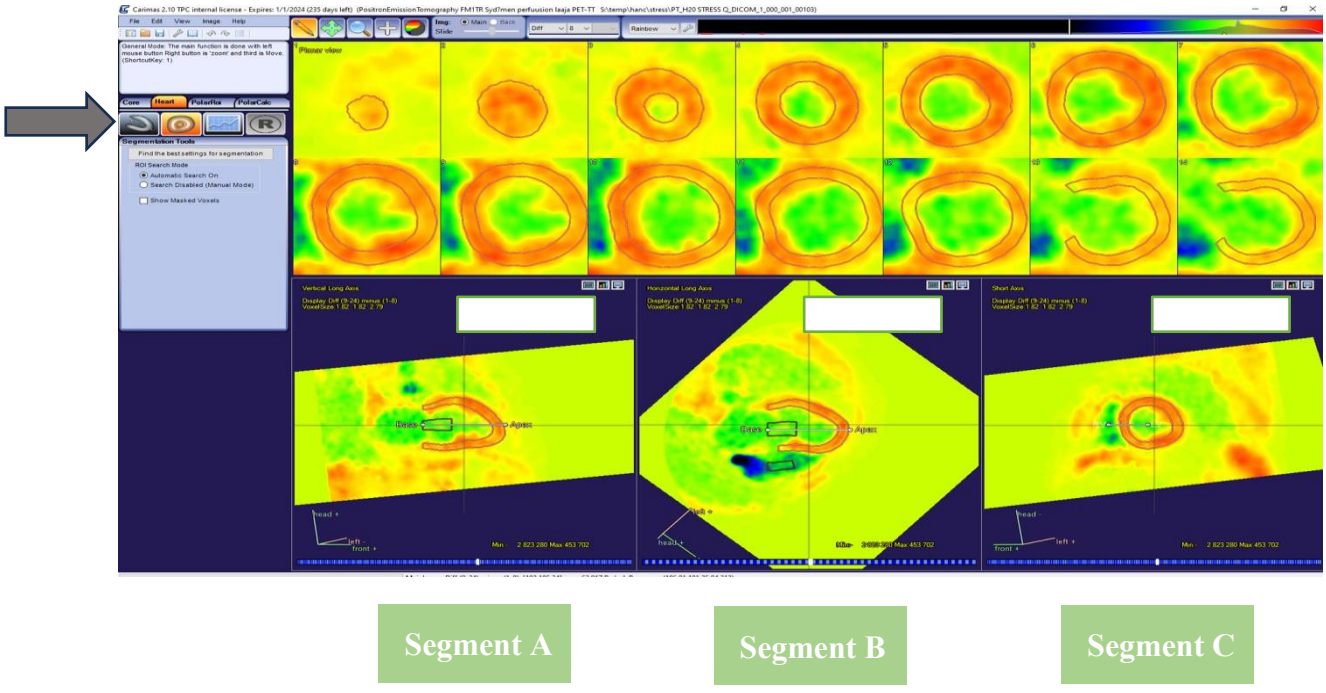


Figure 13. Continuation of segmentation.

So once the segmentation is done, we now “fit” the model for Oxygen-15-labelled water or radiowater as shown in figure 14.

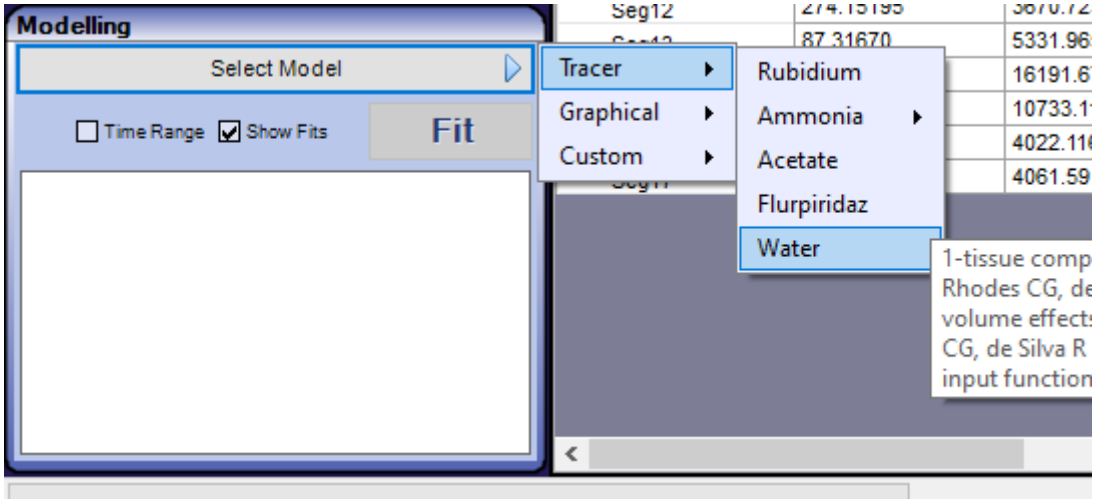


Figure 14. Fitting the radiowater tracer for results.

Once we click on “Fit” we get the results below shown in Figure 15. This displays the polar maps on the top left corner, the MBF data on the botton left corner, in the top right corner we have the time activity curve, and on the bottom right corner we can see the histogram distribution of the polar map that gives is the pixel intensity of the polarmap.

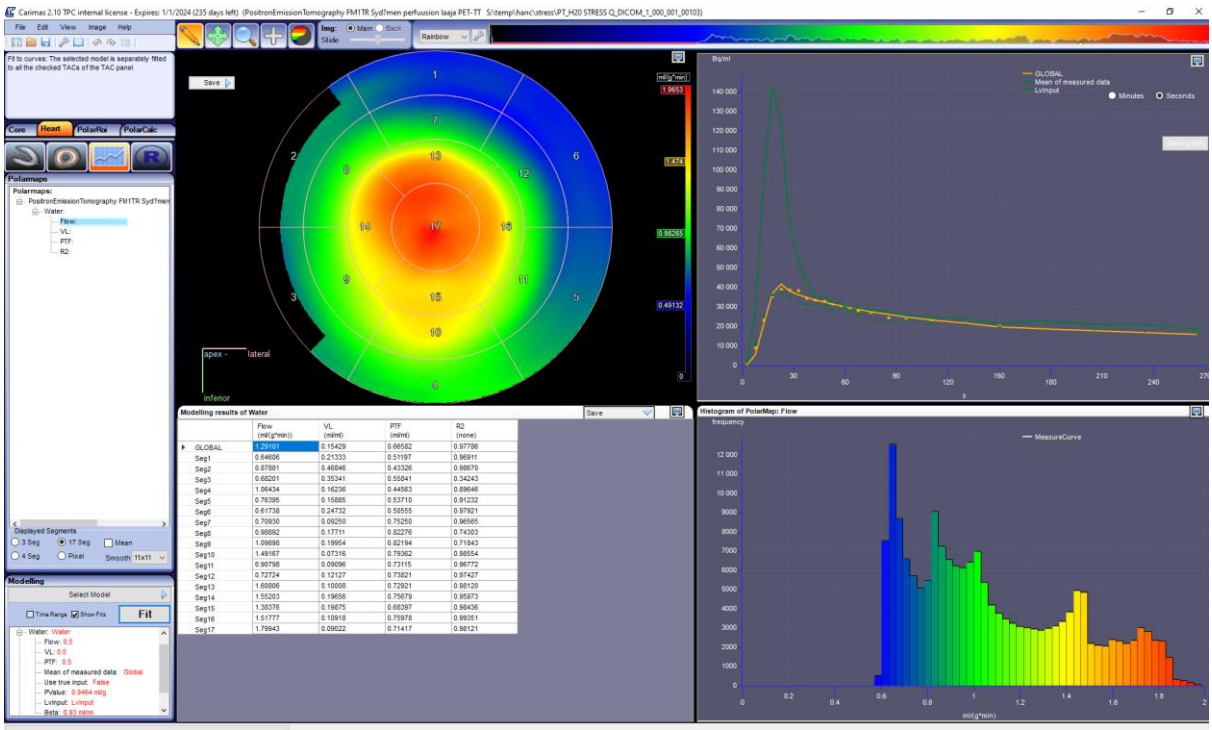

Figure 15. The final results displayed on Carimas after segmentation.

### 4.3.2 Protocol for extracting Histogram

As saving the histogram requires more than a few straightforward steps, we follow the protocol below to extract and save that information.

1. Choose the Polar map: Identify and choose the specific polarmap for which you want the histogram.

2. Open the Polarmap Settings: Access the menu and follow the path Edit > Other commands > Polarmap To Core.

3.Now switch to "Core" view. This will allow you to examine the recently uploaded polarmap in the picture list.

4. To activate the Polarmap, choose the new Polarmap image from the image list and set it as the primary image for analysis.

5. Locate the Visualization Cutpoint: The polarmap, which is usually a two-dimensional picture, may not be immediately visible as it is derived from a preceding three-dimensional image. To determine the cutpoint in the Polarmap, choose picture > find position of maximum when the polarmap is the primary image.

To realign and recentre the display to the highest point inside the polarmap, simply press the x button.

6. To enter Histogram Mode, just click the middle button positioned at the upper right corner of the picture visualization interface.

7. Choose the histogram tool and once it is in histogram mode, enable the histogram analysis tool.

8. Modify Colour Range: Utilise the colour crop tool found in the colour bar. Modify the histogram to include the complete range, excluding any sections that are empty or have zero-value areas.

9. Save the Graph: Click the option to store the histogram graph.

10. Select the .txt format when given, as it is compatible with the histogram plot data.

### 4.3.3 Data obtained

Polar Maps:

Polar maps are created after the process of segmentation in order to visually display the heart. A polar map converts complex three-dimensional cardiac blood flow data into a concise two-dimensional representation. The two-dimensional depiction is especially valuable for evaluating the circulation of blood into and out of the heart muscle, as well as for contrasting various sections of the heart, such as pinpointing areas with impaired blood flow.

MBF data:

The post-segmentation MBF results offer precise information on the blood perfusion in the cardiac muscle. These values are vital for assessing the heart's health, providing insights into possible locations of ischemia or infarction.

VOI Data:

The VOI data, found in the "Core" column of the Carimas program, captures precise locations inside the cardiac pictures for in-depth examination. The advantage of saving the VOI data in .nii format lies in its interoperability with complex image analysis applications. This format is specifically intended to manage datasets with different dimensions and is widely accepted as a standard in the field of medical imaging. It greatly enhances interoperability and accuracy in following analytical procedures.

Histogram:

They are obtained for each polar map by using the segmentation methodology outlined above. The histograms give a visual representation of the distribution of pixel intensity in the polar map of the picture. This is crucial for measuring changes in blood flow inside the heart.

*4.4 Workflow*


Figure 16. Showing the workflow that was incorporated to extract the results

Following the extraction of the data elaborated above, we proceed to the crucial step of consolidating it, during which we methodically categorised and arranged the data we had collected. With the volume of data we have, using coding languages like Python and MATLAB were used, to ensure the precision of our study, as it would provide the groundwork for the next evaluation phase.

Our objective was to provide a seamless and efficient framework of codes for all the different kinds of data we extracted. This systematic strategy would not only assist us in distinguishing data and correlations within them, but also enable us to derive significant insights from the. Our goal was to transform the findings into useful insights that provide a strong basis for decision-making and provide a deeper understanding of the underlying dynamics.

4.4.1 Statistical test

The three main tests we used in this study was the Wilcoxon test to find the significance of the difference and the Dice score and Jaccard Index to identify the similarities.

Wilcoxon Test: It is a non-parametric statistical test that compares two paired groups. We used this in our study since we have two sets of data that are connected in some way, so it's easier to compare them. This test helps us to check if the differences we saw in our data are likely to be significant differences or not.

Jaccard index: This is a statistical test that is used to compare the similarity and the diversity of the sample set. It checks how much these groups have in common compared to how much they differ.

$$\text{Jaccard Index} = \frac{A \cap B}{A \cup B}$$

Equation 1. Formula for Jaccard Index

Dice score: This is a similarity coefficient like Jaccard Index to also guage the similarity between two samples. But the difference is that it calculates the intersection twice unlike in Jaccard Index.

$$\text{Dice score} = \frac{2\ X\ A \cap B}{A + B}$$

Equation 2. Formula for Dice Score

4.4.2 Coding

In this thesis, we used Python and MATLAB's capabilities to organise our data more efficiently.

Initially, a script to properly modify the size of the polar maps, ensuring a consistent dataset for precise classification was created. Following that, the attention was directed towards obtaining MBF measures from the CSV files. We meticulously gathered this data from individuals with diverse backgrounds. In order to assess the significance of differences between these two groups, we employed the Wilcoxon test, which is a non-parametric approach for comparing two paired data without making any assumptions about their distribution.

In order to account for the potential inaccuracies caused by unreliable segments, we conducted a reassessment of the Wilcoxon test by removing segments 2, 3, and 17. The decision was made based on the general understanding that these segments frequently include values that have the

potential to affect and alter our analytical results and decrease their precision. By employing this strategy, we were able to maintain a uniformity in our evaluations and improve the practical significance of our findings. We simultaneously utilised a comprehensive technique to examine Perfusable Tissue Fraction (PTF) data. PTF is a metric that quantifies the extent to which cardiac tissue can be supplied with blood perfusion.

Upon doing an analysis of the histogram data for MBF and PTF, a Python script was developed to overlay the values from both groups. This comparison demonstrated the disparities between both of them visually and quantitatively.

One of the focus of this study was on the VOI. In order to evaluate the degree of alignment between different segmentation results, a script that computes the Dice score was created. This statistic offered an assessment of the extent to which segmented regions were similar. Furthermore, measurements of the VOI volume were extracted in order to determine the potential effects of segmentation changes on volumetric evaluations.

This computational analysis not only enabled us to conduct a comprehensive comparison of segmented images, but also provided us with significant insights into the complexities of cardiac perfusion imaging.

Our research involved the classification of patients into two distinct groups: ischemia and non-ischemic. This categorization was based on a code that takes into account the rate of blood flow. A threshold of 2.3 ml/g/min was set. If the blood flow in adjacent parts of the heart drops below this level, we expect a restricted blood supply, which may indicate probable ischemia.

Figure 17, visually describes the step-by-step functioning of the classification code. This flowchart provides an overview of the sequential steps involved in the decision-making process when our algorithm analyses data from the cardiac segments. By employing this automated decision-making strategy, we are able to maintain fairness in our classification process by depending on predetermined criteria rather than subjective evaluations. Precision and consistency are of utmost importance in diagnosis, since they have a substantial influence on the well-being of patients.

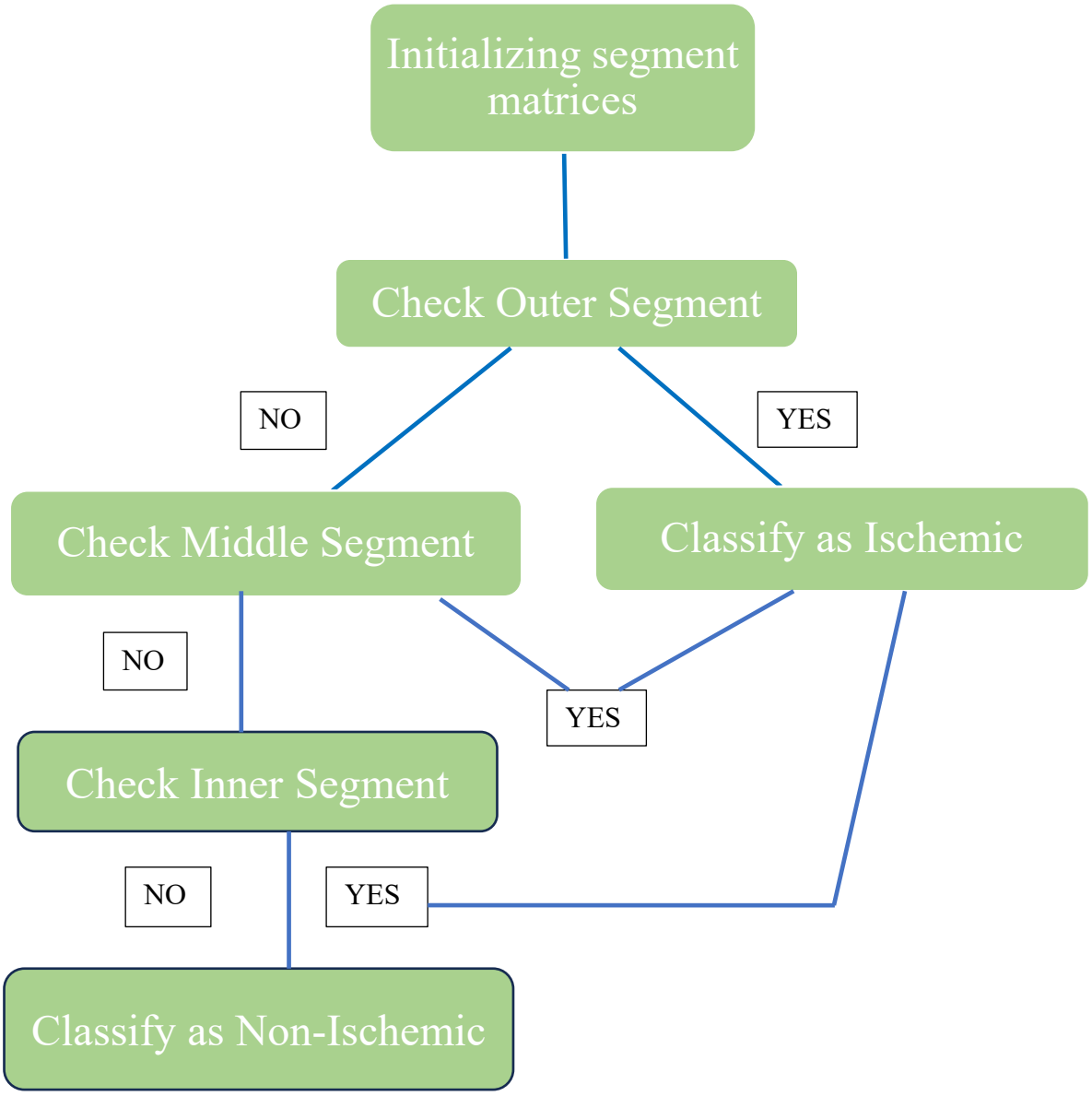


Figure 17. Schematic flow of the classification code. Where ‘yes’ means that it exceeds the 2.3 threshold and ‘no’ means that it does not exceed.

To run our CNN code, we standardized all the polar maps by resizing them uniformly through cropping. This stage ensures that the model consistently examines images by detecting patterns in a systematic manner. After completing the picture preparation process, we employed a Python script to perform k-fold cross-validation. The main parts of this code are shown in figure 18.

```
#MODEL EVALUATION

scores = polar_model.evaluate(X[test], Y[test], verbose=0)
print("%s: %.2f%%" % (polar_model.metrics_names[1], scores[1]*100))


#MODEL COMPILATION

opt = optimizers.SGD(learning_rate=0.005, momentum=0.9)
polar_model.compile(loss=keras.losses.binary_crossentropy, optimizer=opt, metrics=[tf.keras.metrics.AUC()])opt = optimizers.SGD(learning_rate=0.005, momentum=0.9)
polar_model.compile(loss=keras.losses.binary_crossentropy, optimizer=opt, metrics=[tf.keras.metrics.AUC()])


#MODEL TRAINING

polar_train = polar_model.fit(X[train], Y[train], batch_size=batch_size, class_weight=weights, epochs=epochs, verbose=2, shuffle=True)



#MODEL DEFINITION

polar_model = Sequential()
polar_model.add(Conv2D(12, kernel_size=(3, 3), strides=(2,2), activation='relu', input_shape=(x_y_size_images,x_y_size_images,3), padding='same'))
polar_model.add(MaxPooling2D((2, 2)))
polar_model.add(Conv2D(16, kernel_size=(3, 3), strides=(2,2), activation='relu', padding='same'))
polar_model.add(MaxPooling2D((2, 2)))
polar_model.add(Conv2D(32, kernel_size=(3, 3), strides=(2,2), activation='relu', padding='same'))
polar_model.add(MaxPooling2D((2, 2)))
polar_model.add(Conv2D(64, kernel_size=(3, 3), strides=(2,2), activation='relu', padding='same', kernel_regularizer=regularizers.l2(0.1)))
polar_model.add(MaxPooling2D((2, 2)))
polar_model.add(Flatten())
polar_model.add(Dense(512, activation='relu'))
polar_model.add(Dense(128, activation='relu'))
polar_model.add(Dense(number_of_outputs, activation='sigmoid'))
```

Figure 18. A snapshot of all the important parts of the CNN code.

# 5 RESULTS

## *5.1 Medical vs Non-Medical Expert*

In this study we reviewed the results from 44 patients from both medical and non-medical backgrounds. The task involved the examination of Polarmap images, data on MBF, and measures of VOI.

In the following part, we will dissect the results that were obtained from each one of these results and investigating their connections and reflecting on the implications they provide about heart health.

### 5.1.1 Polar Maps

A polar map is a visual aid that allows us to track the blood flow to the heart muscle and assess its efficiency in supplying it to the myocardium. By mapping the perfusion patterns in the heart, we have the capacity to readily detect locations where blood flow may be impaired. This is vital for recognizing regions of ischemia.

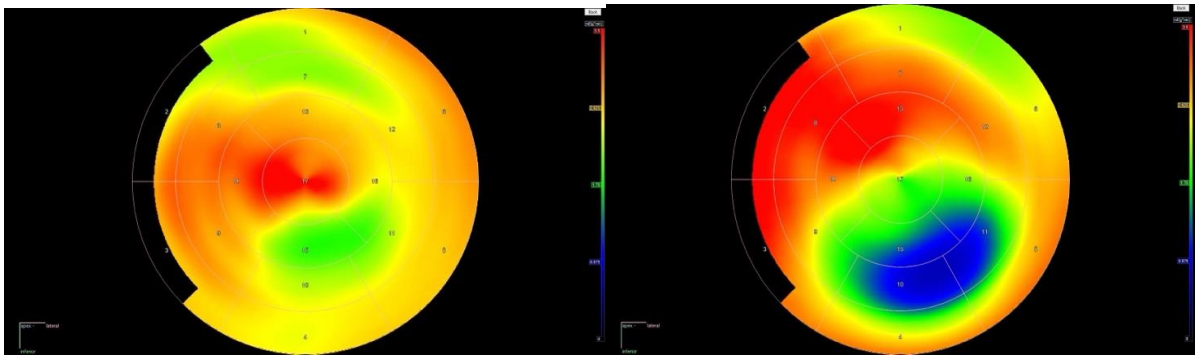

Figure 19. Patient 031 medical vs non-medical

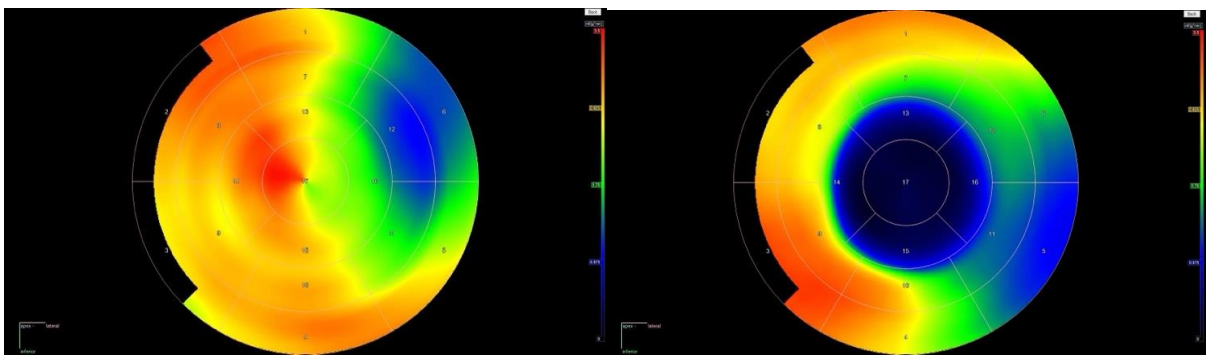

Figure 20.Patient 036 medical vs non-medical

In figure 19 and 20, the images we have analysed clearly showcases how various segmentation techniques can result in producing different polar maps. These differences go beyond technicality as they carry significant implications for evaluating cardiac function in a clinical setting. The accuracy and precision in developing these maps can significantly influence the diagnostic process and ultimately determine the efficacy of patient outcomes.

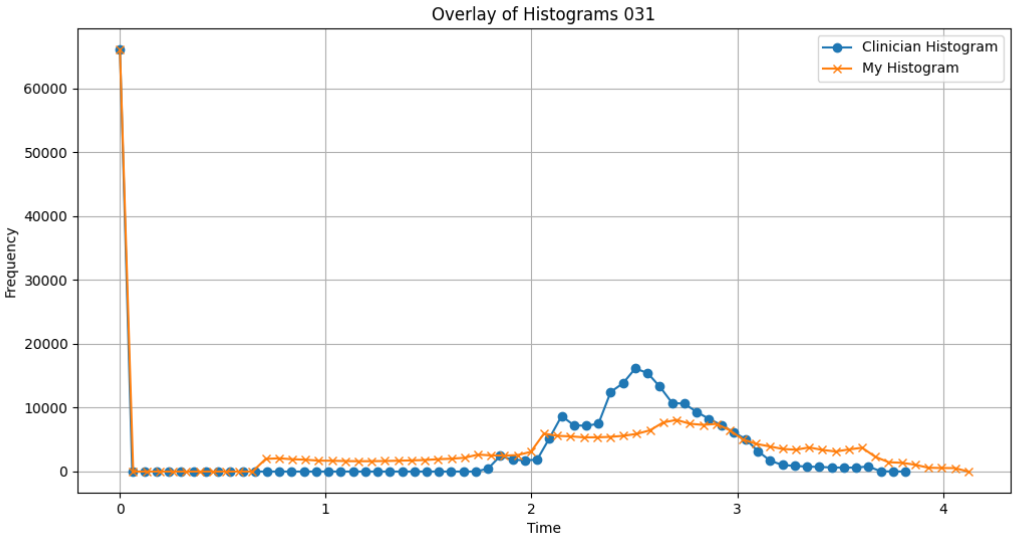


Figure 21. Histogram of patient 031

What we have here in figure 21 and figure 22 is essentially a representation of the polar map on histograms, which helps to display the nuances of pixel intensity in a clear way. This approach allows us to assess segmented pictures in terms of both visual appearance and numerical measurements. This approach allows us to assess segmented pictures in terms of both visual appearance and numerical measurements.

By examining the histogram we can notice differences in pixel intensity across various parts of the polar map indicating diverse perfusion levels within the heart muscle. This thorough analysis is crucial for pinpointing areas of concern such as regions, with blood flow and offers a detailed comparative perspective that assists in assessing the same effectively.

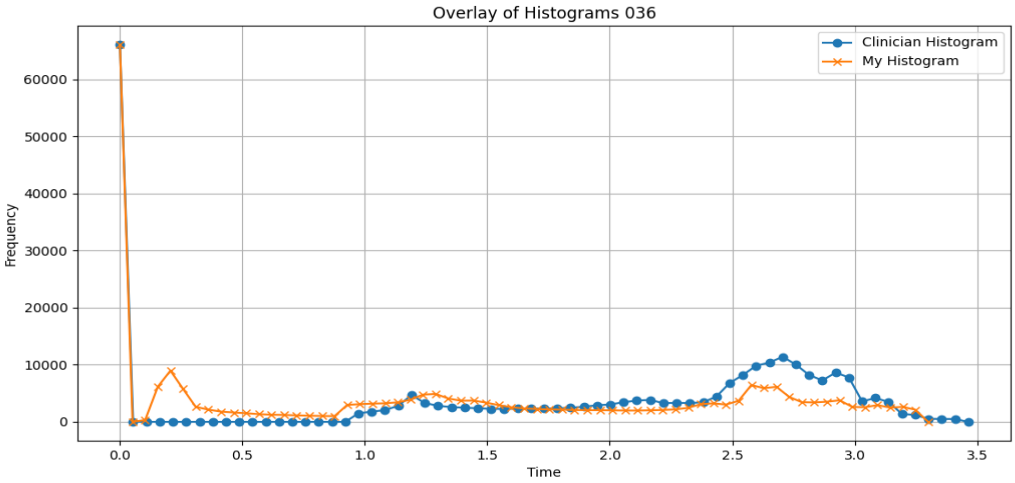


Figure 22. Histogram of patient 036

### 5.1.2 MBF Data

The MBF values extracted from the segmentation were also compared. And the values within the red boundaries show us how different the values are when comparing it between figure 23 and figure 24.

```
•Region;Flow;VL;PTF;R2
Units;ml/(g*min);ml/ml;ml/ml;none
GLOBAL;3.88069296679502;0.0331886252950582;0.999999999999995;0.990545940021903
Seg1;3.38568066543669;0.114595780117744;0.963100944458351;0.98848462314891
Seg2;2.20865139049066;0.333780031375727;0.764839413185998;0.970933719838087
Seg3;2.58899058358683;0.342269712438612;0.81037949885416;0.971929264544883
Seg4;3.95415452692945;0.052938930063837;0.999999999999999;0.952667538654528
Seg5;3.79105130709955;0.0765147043799288;0.999999999999999;0.977415528484587
Seg6;2.97759056344932;0.0344453954442777;1;0.981596026192069
Seg7;3.59848947262588;0.0339758230790573;0.990032313449403;0.982251302800134
Seg8;2.65589593572313;0.333839447728025;0.694950619525945;0.972634926398261
Seg9;3.25660914834003;0.368968247526555;0.706407799967639;0.966433812473206
Seg10;4.4431666100837;6.22586151074338E-16;0.999999999999998;0.940178129766387
Seg11;3.91302278746528;0.0322977942631643;1;0.958196658358127
Seg12;3.10569668970923;0.0426807013898633;0.999999999997784;0.977834008580865
Seg13;3.23670242784395;2.18332021899277E-16;0.996376635605925;0.983186689289803
Seg14;3.34949620012936;0.259137877293523;0.802549211157632;0.971430650731862
Seg15;3.73084736984948;0.0657954949418678;1;0.945501799547398
Seg16;3.46890561225764;0.00545317991657214;0.999999999999999;0.963948227418249
Seg17;4.51885671896143;1.12103269916559E-15;0.992959937942706;0.961834083163118
LAD;3.82792783048801;0.0750750633444984;0.939934511592934;0.991813673532776
LADwa;3.24018805749789;0.146653677993849;0.892239562970027;0.995031912700927
LCX;3.43170290876429;0.0350383605165613;1;0.983958389993989
RCA;4.03945455796508;0.067918714732243;0.994953000484206;0.968946551887831

```

Figure 23. The MBF values of patient 001 by a Non-Medical background individual.

```
•Region;Flow;VL;PTF;R2
Units;ml/(g*min);ml/ml;ml/ml;none
GLOBAL;3.28844;0.106081;0.933128;0.987954
Seg1;2.80981;0.117878;0.956078;0.982335
Seg2;1.75924;0.35734;0.726989;0.982802
Seg3;1.84578;0.444013;0.731045;0.976811
Seg4;2.54991;0.29995;0.861056;0.978805
Seg5;3.00662;0.12428;1;0.983775
Seg6;2.66607;0.0907501;1;0.995141
Seg7;3.08616;0.0581964;1;0.981706
Seg8;2.64105;0.252212;0.763693;0.990181
Seg9;2.42973;0.450758;0.641298;0.975204
Seg10;3.44102;0.166394;0.929309;0.962479
Seg11;4.23824;0.0468186;1;0.933492
Seg12;3.11679;0.0889703;1;0.972595
Seg13;2.82873;0.00421132;1;0.979317
Seg14;2.91605;0.11404;0.884234;0.987576
Seg15;3.6489;0.0968316;1;0.947593
Seg16;4.00056;5.49163E-05;1;0.945072
Seg17;4.46652;1.76656E-17;0.946846;0.941797
LAD;3.40202;0.0688842;0.923454;0.984063
LADwa;2.83804;0.0990634;0.934756;0.995215
LCX;3.33988;0.0668876;1;0.983903
RCA;2.82916;0.28021;0.83861;0.979418

```

Figure 24. MBF Values of patient 001 by a Medical background individual.

In order to analyse the differences between our two data sets, we used the Wilcoxon test for this purpose. By analysing the p values produced by this test, we are effectively assessing the likelihood that the patterns detected in the data are due to random chance. We set our standard for determining significance at a p-value of 0.05 or below.

Here in the method we tested, we omitted segments 2, 3, and 17 in one of our comparisons. Before making this modification, we found that 14 patients displayed p values of 0.05 or below, indicating significant patterns in their data. And 12 patients had low p values when the three segments were excluded. After removing the data components that might impact our accuracy, we still find strong evidence indicating a large variance across these individuals.

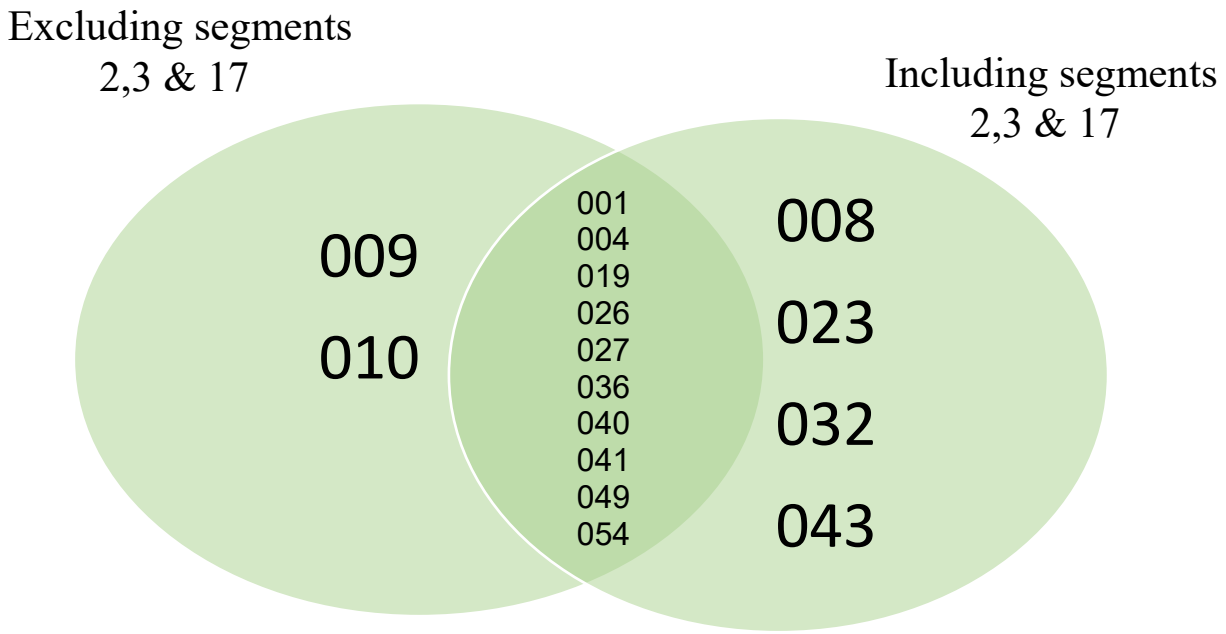


Figure 25. Showing the common 10 patients from both the sets that had a p-value of 0.05 and below.

### 5.1.3 VOI data

In addition, we made a comparison of the VOI, which involved analysing the heart's perfusion. The results were stored in a 3-D volume format. In order to assess the degree of similarity, we adopted the Dice Score and Jaccard Index.

• Result of Dice Score:

There are 24 patients whose values lie within the range of 0.6-0.8, which suggests a modest level of overlap.

There are 20 patients with a score below 0.6, which indicates a very low level of similarity.

• Result of Jaccard Index:

Most patients lie within the 0.2-0.6 range exhibiting a few similarities among the VOIs.

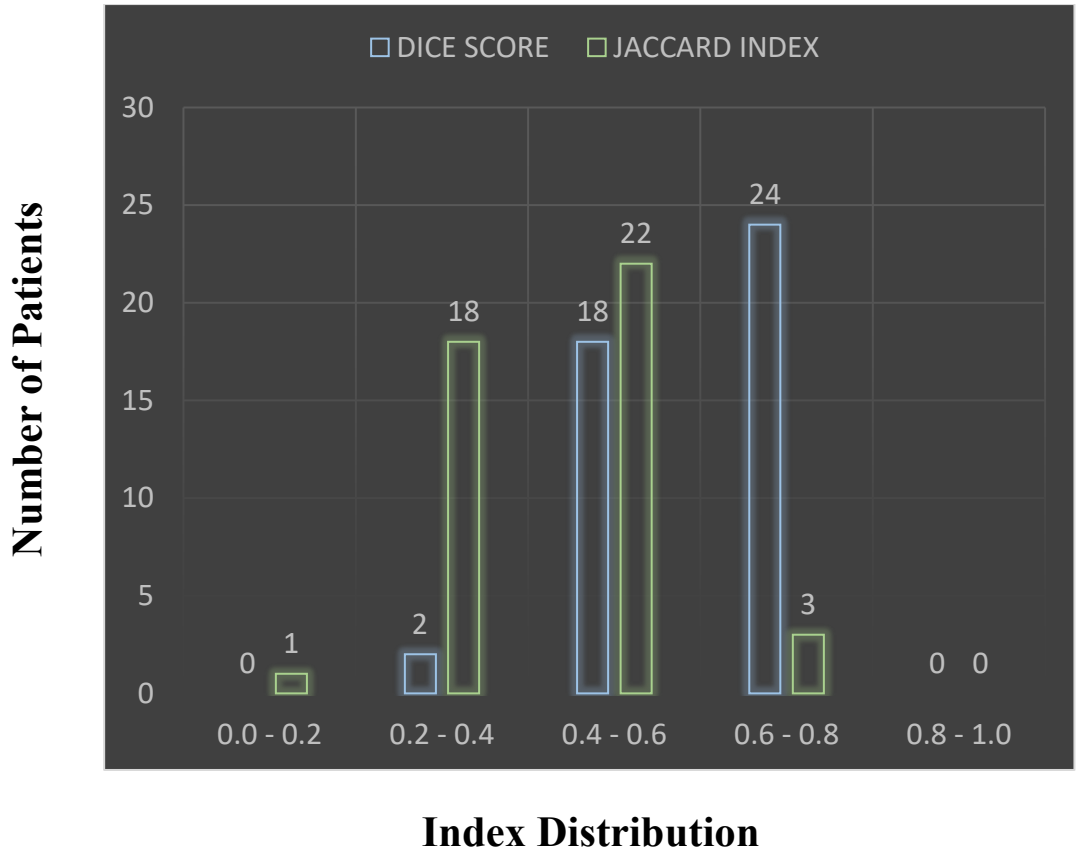


Figure 26. Dice score and Jaccard index result comparison.

## *5.2 Classification results*

Based on the ground truth, it was determined that 23 out of the 55 patients are ischemic. After excluding 11 patients with noisy images, our analysis now focused on a total of 44 individuals, out of which 19 have been diagnosed with ischemic conditions.
Given that the threshold value for ischemia stress MBF is 2.3ml/g/min, we found out that-

• For the individual with a medical background: There were 20 cases classified as ischemic. A total of 17 patients were accurately classified.
• For the individual without a medical background: There were 24 cases classified as ischemic. A total of 17 patients were accurately classified.

An interesting finding is that patient 016 shows ischemiac symptoms, however was not categorised as ischemic in both of the datasets.

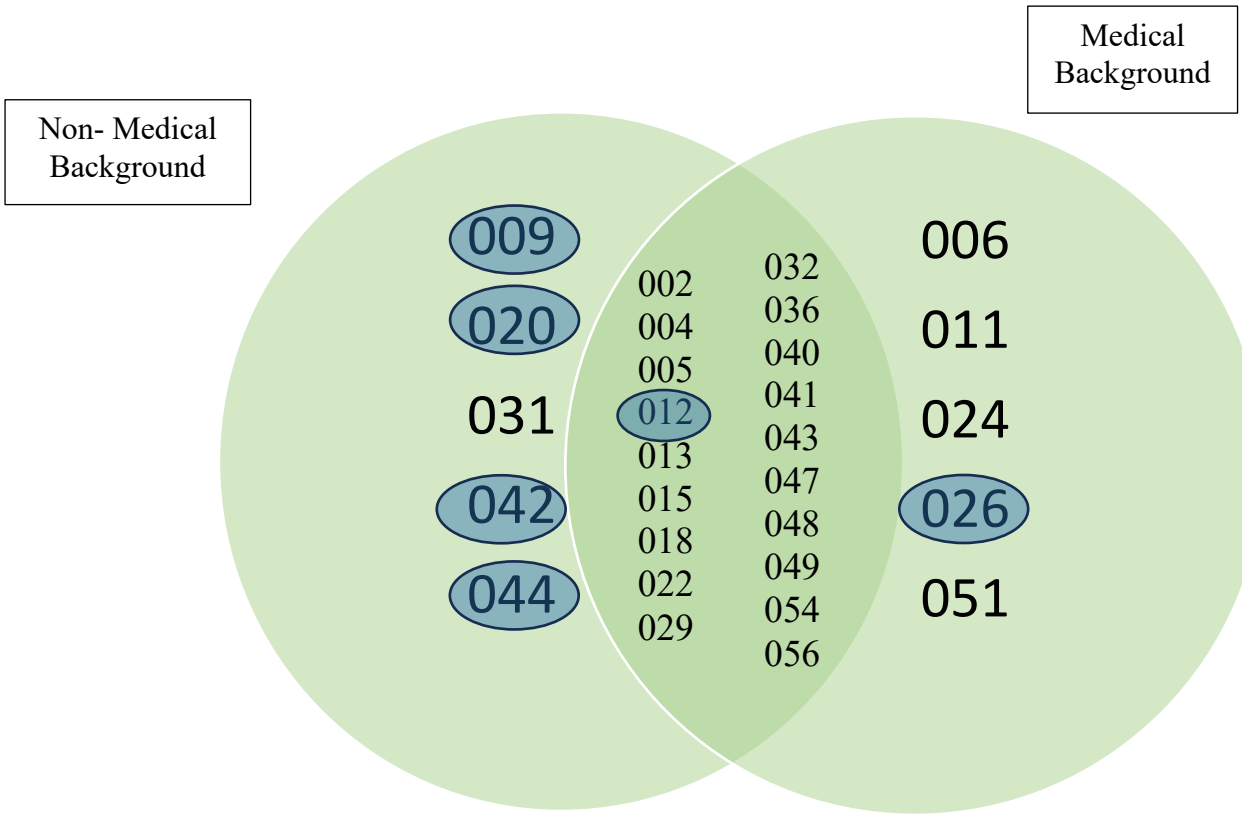


Figure 27. Venn diagram of the classified patients from both the sets.

From figure 27, the Venn diagram shows that based on the classification result, there were 19 patients who were identified by both individual with a medically trained background and individual without a medical background.

The patients marked in blue are those who are non-ischemic but have been misclassified as ischemic using a threshold of 2.3 ml/g/min on the MBF data acquired from the segmentation method.

## *5.3 K- fold results*

During the examination of our CNN model result, we evaluated the accuracy and used the K-fold cross validation method to examine the difference in the results. The technique was systematically performed on 10, 5, and 3 folds to examine the AUC values of the model. After understanding the variations of the values we got using statistical measurements such as mean, median, and standard deviation we found that the 3-fold and 5-fold validations results showed better results in comparison to the 10-fold validation. As a result of this discovery, we decided to focus our analysis and discussion just on these two folds as it was offering us an accurate assessment of its performance with new data.

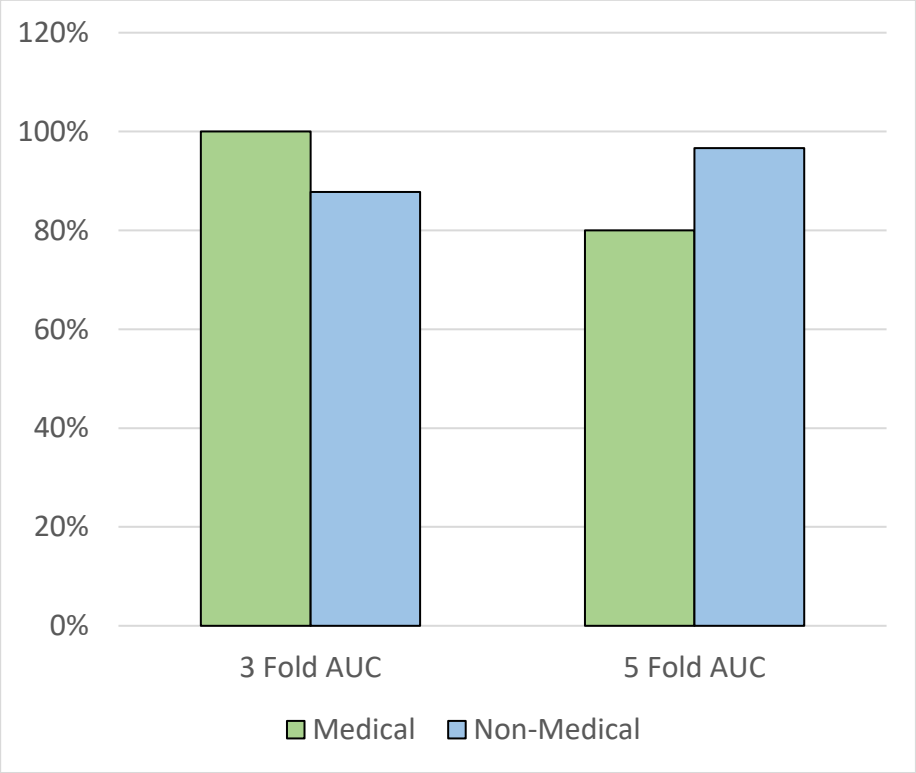


Figure 28. Comparison between the AUC result for normal K-fold

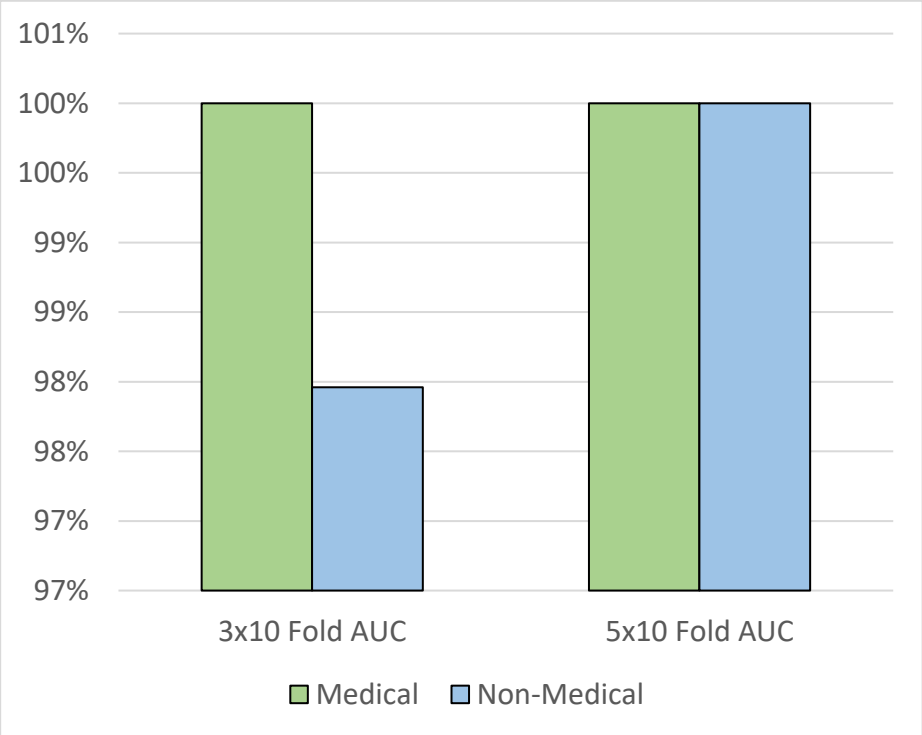


Figure 29. Comparison between the AUC result for repeated K-fold

In the tables 1, 2, 3 and 4 below, we have incorporated the different results of our CNN model when subjected to different folds. The tables display AUC values that indicate the model's performance. In addition, we also have the mean, median and standard deviation, which effectively indicate the central value, middle value, and divergence from the mean.

Organizing all this data in tables helps us to compare and better understand the model's outcomes as we modify the number of folds. It is similar to providing the model with many sets of practice exams and seeing which one best prepares it for real-world applications. This is crucial to make sure that our model is well-prepared and reliable for use cases such as helping clinicians in making decisions based on its predictions.

| | AUC | Mean | Median | Standard Deviation |
|---|---|---|---|---|
| Normal 3 Fold Medical | 100% | 91.80% | 97.73% | +/- 10.03% |
| Normal 3 Fold Non-medical | 87.76% | 90.56% | 87.76% | +/- 6.85% |

Table 1. Comparison between medical and non-medical background 3 fold.

| | AUC | Mean | Median | Standard Deviation |
|---|---|---|---|---|
| Normal 5 Fold Medical | 80% | 85.84% | 96.43% | +/- 16.69% |
| Normal 5 Fold Non-medical | 96.67% | 91% | 96.67% | +/- 11.52% |

Table 2. Comparison between medical and non-medical background 5 fold.

| 10 repeats | AUC | Mean | Median | Standard Deviation |
|---|---|---|---|---|
| Repeated 3 Fold Medical | 100% | 91.67% | 93.52% | +/- 8.43% |
| Repeated 3 Fold Non-medical | 97.96% | 90.35% | 89.14% | +/- 8.26% |

Table 3. Comparison between medical and non-medical background repeated 3 fold.

| 10 repeats | AUC | Mean | Median | Standard Deviation |
|---|---|---|---|---|
| Repeated 5 Fold Medical | 100% | 89.94% | 93.93% | +/- 12.20% |

| | | | | |
|---|---|---|---|---|
| Repeated 5 Fold Non-medical | 100% | 91.36% | +/- 11.08% | 100% |

Table 4. Comparison between medical and non-medical background repeated 5 fold.

# 6 DISCUSSION

In addition to the results section, we observed certain occurrences and examples during separate tests. These examples provided us with valuable insights and improved our understanding of the correlation. These additional tests are not crucial but it added some insight and provided us with some patterns that we may have missed. By considering these tests, we can strengthen our research and ensure that no essential information is overlooked. By integrating our results with these supplementary assessments, we may obtain a comprehensive outlook on our study objectives which makes it more trustworthy and gives us relevant conclusions that can be applied.

To classify ischemia, we allocated a numerical value of 1 to segments exhibiting evidence of ischemia, while segments without such indications were given a numerical value of 0. This straightforward grading method allowed us to accurately differentiate between non-ischemic regions.

*Ischemic Segments for Patient 026: [1. 1. 1. 0. 0. 0. 0. 1. 0. 0. 0. 0. 0. 0. 0. 0. 0.]*
*Ischemic Segments for Patient 020: [1. 1. 0. 0. 0. 0. 1. 1. 0. 0. 0. 0. 0. 0. 0. 0. 0.]*

Examining patients 020 and 026 as an illustration. At first, both individuals were categorised as having ischemia when we evaluated all 17 segments of the polar map. However, this changed when we eliminated the three segments, 2, 3, and 17. In the absence of these segments, both individuals were classified as non-ischemic. This emphasises a key point- the adjacent sections showing indications of ischemia might have a major influence on the overall diagnosis. Patient 026 had distributed ischemia segments, with initial involvement of segments 1, 2, and 3, followed by a separate segment 8. However, patient 020 had a same initial pattern but afterwards experienced ischemia in segments 7 and 8.

This finding highlights the need of taking into account several criteria when diagnosing ischemia. The presence of ischemic signals in nearby segments can significantly impact its classification. Our study methodology illustrates how analysing segments may offer a comprehensive understanding of the patients' condition, potentially impacting their approach to therapy.

Table 5 below provides an analysis that examines the significance of variations across different segments of the heart. This analysis focuses on the p value, which is a statistical measure used in Wilcoxon test to determine if observed differences. We considered a p-value equal to or less than 0.05 to be statistically significant.

None of the patients exhibited measurements within the specified range for segments including LAD, LADwa, LCX and RCA. This suggests that there were no noteworthy variances in measurements or observations among individuals in these particular segments. But for the PTF values, 15 patients had a p value of less than 0.05 and that became 14 patients when segment 2,3 and 17 were excluded.

| | PTF | 4 segment |
|---|---|---|
| Included | 15 patients | 0 patients |
| Excluded | 14 patients | 0 patients |

Table 5. PTF and 4 Segments results.

In Figure 30, we can see the scatter plot to visually compare the VOI volumes among the group of patients between the medical and non-medical background. It is evident that the quantities differ across patients. An interesting observation is that patients 021 and 046 have the same VOI volumes making them outliers in a dataset where each patients VOI volume is unique.

Furthermore when we examine the group as a whole we notice a division in how these volumes differ. There is a subgroup of 21 patients where the difference in VOI volumes are minimal indicating that while there are variations they are not significantly different. On the other hand, the remaining 21 patients shows good differences in their VOI volumes. These variations are significant enough to investigate more to understand their underlying causes.

This type of analysis plays a role in identifying patterns or irregularities, in medical imaging data, which can impact diagnosis and treatment decisions. It also highlights the diversity within populations and emphasises the importance of considering individual characteristics when assessing medical images.

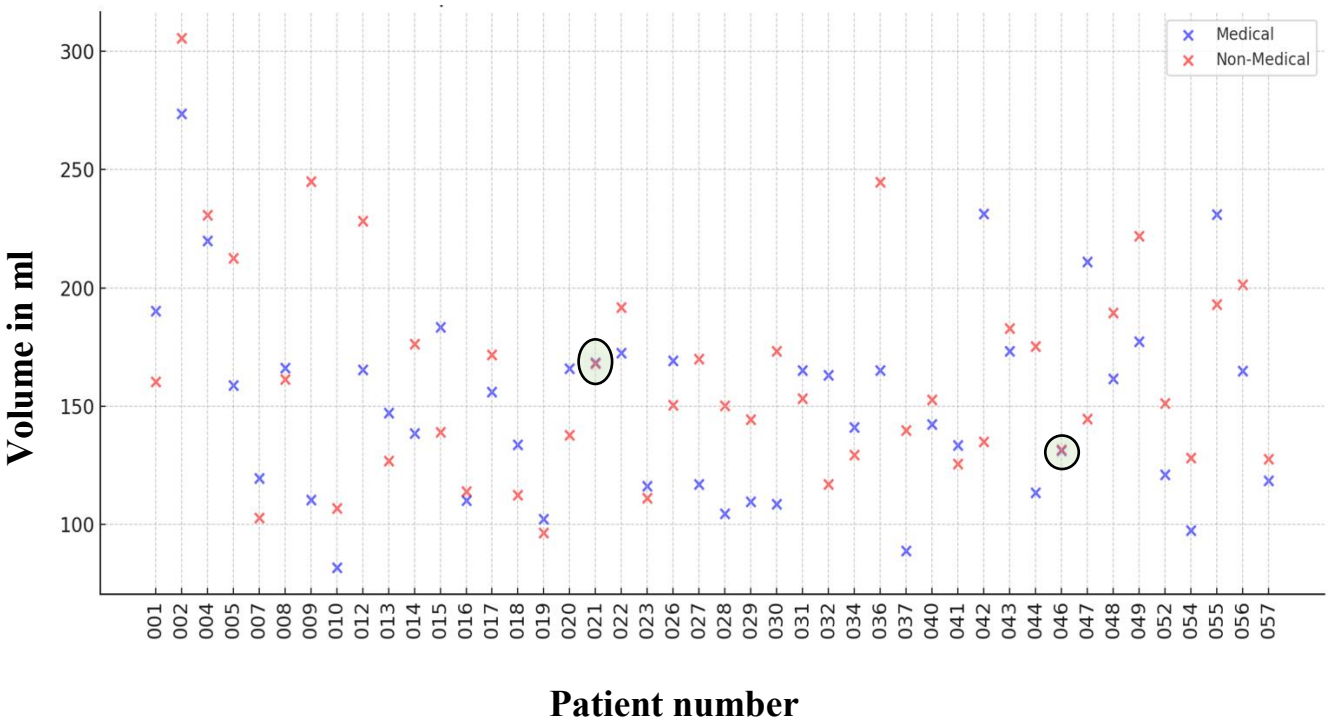


Figure 30. Scatter plot of VOI volumes between Medical Individual and Non-Medical Individuals.

## *6.1 Future studies*

Although these are promising evidences in our study, it is essential to use a systematic strategy. In order to enhance our understanding and properly assess the importance of our findings, a bigger dataset is required. From that, we may improve the validity of our results while getting a better understanding of their correctness. This step is crucial before applying technology in the healthcare sector.

DL has shown potential in analysing quantitative cardiac perfusion polar maps. It greatly enhances our ability to identify individuals who are at risk of experiencing negative cardiovascular events. The power of DL not only resides in its performance, but it also surpasses basic ML algorithms that consider clinical, functional, and flow related elements [43].

However, we are only exploring the superficial aspects. Further investigation is required to fully understand the practical significance of DL estimations in evaluating the risk of

myocardial ischemia in patients. The potential for customization and enhancement of patient care is the driving force behind our ongoing research.

# CONCLUSION

Our study finds that there are noticeable differences in our results. We can see it in the visual representation of polar maps, histograms, VOI data, and MBF data after segmentation of the images. This suggests that an individual's expertise and background has an impact on the resultant images produced.

Significantly, by utilizing the classification technique with a threshold of 2.3 ml/g/min, we accurately categorised a total of 17 cases from individuals from both the backgrounds. This indicates that these differences do not significantly affect in the final prediction of ischemia.

It is important to note that automated solutions have not yet been widely accepted due to the complexity that always exists when segmenting medical images. Although computers and algorithms have their advantages, they are unable to completely substitute the expertise of a human professional [3].

Our CNN model constantly demonstrate great performance, independent of the creator of the polar maps. The CNN routinely achieves outstanding accuracy levels, ranging from 85% to 100%. This shows that the degree of reliability is quite encouraging, suggesting that the CNN approach has the potential to significantly impact image classification.

However, despite these favourable indications, it is crucial to approach this situation with a measure of caution. In order to ensure the strength and relevance of our findings, it is important to evaluate this using an adequate dataset. Expanding the dataset would enhance the credibility of the findings and offer insights into its truthfulness. Before diving into applications within the field of medicine, this confirmation step is of extreme significance so we can approach the incorporation of modern technology into regular medical practices.

## ACKNOWLEDGEMENT

The completion of this thesis would not be possible without my supervisors. I am deeply grateful to Dr. Jarmo Teuho and Prof. Riku Klén for their mentorship and constant support over this past year. Their expertise and valuable input have been fundamental in my research and professional development.

I also owe Turku PET Centre and Turku University Hospital (TYKS) for giving me the opportunity to learn and be a part of something so valuable.

I also want to express my appreciation to my parents. Their unwavering belief in me and continuous encouragement has motivated me to persevere and achieve my goals.

I am appreciative of the powerful AI tools, ChatGPT and Quillbot, that have been helpful in improving the clarity and fluency of my writing.

Lastly, I want to thank the team at the BIMA department at the University of Turku and Åbo Akademi University. The excellent academic environment and collaborative spirit within have been vital for my growth as a researcher. Moreover, I am thankful for the friendship, intellectual conversations and meaningful exchanges with my peers and group members.

## REFERENCES


1. Juarez-Orozco, L. E., Martinez-Manzanera, O., Storti, A. E. & Knuuti, J. Machine learning in the evaluation of myocardial ischemia through nuclear cardiology. Curr. Cardiovasc. Imag. Rep.12, (2019).
2. Slart RHJA, et al. Position paper of the EACVI and EANM on artificial intelligence applications in multimodality cardiovascular imaging using SPECT/CT, PET/CT, and cardiac CT. Eur. J. Nucl. Med. Mol. Imag. 2021;48:1399–1413. doi: 10.1007/s00259-021-05341-z. - DOI - PMC - PubMed
3. Teuho, J., Schultz, J., Klén, R., Knuuti, J., Saraste, A., Ono, N., & Kanaya, S. (2022). Classification of ischemia from myocardial polar maps in 15O-H2O cardiac perfusion imaging using a convolutional neural network. *Scientific reports*, *12*(1), 2839. https://doi.org/10.1038/s41598-022-06604-x
4. J. Teuho and R. Klén, "Seyedmohammadreza Hosseini".
5. Basu S, Kwee TC, Surti S, Akin EA, Yoo D, Alavi A. Fundamentals of PET and PET/CT imaging. Ann N Y Acad Sci. 2011 Jun;1228:1-18. doi: 10.1111/j.1749-6632.2011.06077.x. PMID: 21718318.
6. Okrainec K, Banerjee DK, Eisenberg MJ. Coronary artery disease in the developing world. American heart journal. 2004 Jul 1;148(1):7-15.
7. Shimokawa H, Yasuda S. Myocardial ischemia: current concepts and future perspectives. Journal of cardiology. 2008 Oct 1;52(2):67-78.
8. Gaziano TA, Bitton A, Anand S, Abrahams-Gessel S, Murphy A. Growing epidemic of coronary heart disease in low-and middle-income countries. Current problems in cardiology. 2010 Feb 1;35(2):72-115.
9. Megna, R., Petretta, M., Assante, R., Zampella, E., Nappi, C., Gaudieri, V., Mannarino, T., D'Antonio, A., Green, R., Cantoni, V., Arumugam, P., Acampa, W., & Cuocolo, A. (2021). A Comparison among Different Machine Learning Pretest Approaches to Predict Stress-Induced Ischemia at PET/CT Myocardial Perfusion Imaging. *Computational and mathematical methods in medicine*, *2021*, 3551756. https://doi.org/10.1155/2021/3551756
10. Juarez-Orozco, L. E., Knol, R. J. J., Sanchez-Catasus, C. A., Martinez-Manzanera, O., van der Zant, F. M., & Knuuti, J. (2020). Machine learning in the integration of simple variables for identifying patients with myocardial ischemia. *Journal of nuclear*

*cardiology : official publication of the American Society of Nuclear Cardiology*, *27*(1), 147–155. https://doi.org/10.1007/s12350-018-1304-x

11. Seetharam, K., & Min, J. K. (2020). Artificial Intelligence and Machine Learning in Cardiovascular Imaging. *Methodist DeBakey cardiovascular journal*, *16*(4), 263–271. https://doi.org/10.14797/mdcj-16-4-263
12. Abdulhamit Subasi and Riku Klèn "Muhammad Hassan Nawaz".
13. Iida H, Kanno I, Takahashi A, et al: Measurement of absolute myocardial blood flow with H215O and dynamic positron-emission tomography. Strategy for quantification in relation to the partial-volume effect. Circulation 78:104-115, 1988. https://doi.org/10.1161/01.CIR.78.1.104
14. 14.G. Litjens et al., "A survey on deep learning in medical image analysis," Med Image Anal, vol. 42, pp. 60–88, Dec. 2017, doi: 10.1016/j.media.2017.07.005.
15. Maaniitty, T., Knuuti, J., & Saraste, A. (2020). 15O-Water PET MPI: Current Status and Future Perspectives. *Seminars in nuclear medicine*, *50*(3), 238–247. https://doi.org/10.1053/j.semnuclmed.2020.02.011
16. Shin HC, Roth HR, Gao M, Lu L, Xu Z, Nogues I, Yao J, Mollura D, Summers RM. Deep convolutional neural networks for computer-aided detection: CNN architectures, dataset characteristics and transfer learning. IEEE transactions on medical imaging. 2016 Feb 11;35(5):1285-98.
17. "Cardiovascular disease deaths and disparities increased in 2020 | NHLBI, NIH," Jun. 28, 2021. https://www.nhlbi.nih.gov/news/2021/cardiovascular-disease-deaths-and-disparitiesincreased-2020 (accessed Apr. 06, 2023).
18. J. Teuho, J. Schultz, R. Klén, A. Saraste, N. Ono, and S. Kanaya, "Comparison of 12 Machine Learning Methods for Polar Map Classification in Cardiac Perfusion PET," in 2021 IEEE Nuclear Science Symposium and Medical Imaging Conference (NSS/MIC), IEEE, 2021, pp. 1–3.
19. deKemp RA, Renaud JM, Klein R, et al: Radionuclide tracers for myocardial perfusion imaging and blood flow quantification. Cardiol Clin 34:37-46, 2016. https://doi.org/10.1016/j.ccl.2015.08.001
20. Patel MR, Peterson ED, Dai D, Brennan JM, Redberg RF, Anderson HV et al. Low diagnostic yield of elective coronary angiography. N Engl J Med 2010;362:886–95.
21. Montalescot G, Sechtem U, Achenbach S, Andreotti F, Arden C, Budaj A et al.; Task Force Members. ESC Committee for practice guidelines, document re- viewers. 2013 ESC guidelines on the management of stable coronary artery dis- ease: the Task Force

on the management of stable coronary artery disease of the European Society of Cardiology. Eur Heart J 2013;34:2949–3003.

22. Camici PG, D'amati G, Rimoldi O. Coronary microvascular dysfunction: mechan- isms and functional assessment. Nat Rev Cardiol 2015;12:48–62.
23. Crea F, Camici PG, Bairey Merz CN. Coronary microvascular dysfunction: an up- date. Eur Heart J 2014;35:1101–11.
24. Stenström, I., Maaniitty, T., Uusitalo, V., Pietilä, M., Ukkonen, H., Kajander, S., Mäki, M., Bax, J. J., Knuuti, J., & Saraste, A. (2017). Frequency and angiographic characteristics of coronary microvascular dysfunction in stable angina: a hybrid imaging study. *European heart journal. Cardiovascular Imaging*, *18*(11), 1206–1213. https://doi.org/10.1093/ehjci/jex193
25. E. P. V. Le, Y. Wang, Y. Huang, S. Hickman, and F. J. Gilbert, "Artificial intelligence in breast imaging," Clinical radiology, vol. 74, no. 5, pp. 357–366, 2019. [10]
26. F. Al-Turjman, M. H. Nawaz, and U. D. Ulusar, "Intelligence in the Internet of Medical Things era: A systematic review of current and future trends," Computer Communications, vol. 150, pp. 644–660, Jan. 2020, doi: 10.1016/j.comcom.2019.12.030. [11]
27. A. Esteva et al., "A guide to deep learning in healthcare," Nature medicine, vol. 25, no. 1, pp. 24–29, 2019.
28. H.-C. Shin et al., "Deep convolutional neural networks for computer-aided detection: CNN architectures, dataset characteristics and transfer learning," IEEE transactions on medical imaging, vol. 35, no. 5, pp. 1285–1298, 2016.
29. R. Yamashita, M. Nishio, R. K. G. Do, and K. Togashi, "Convolutional neural networks: an overview and application in radiology," Insights into imaging, vol. 9, pp. 611–629, 2018.
30. Ghosh N, Rimoldi OE, Beanlands RS, Camici PG. Assessment of myocardial ischaemia and viability: role of positron emission tomography. European heart journal. 2010 Dec 1;31(24):2984-95.
31. Juarez-Orozco LE, Martinez-Manzanera O, Storti AE, Knuuti J. Machine learning in the evaluation of myocardial ischemia through nuclear cardiology. Current Cardiovascular Imaging Reports. 2019 Feb;12(2):1-8.
32. Gomez J, Doukky R. Artificial intelligence in nuclear cardiology. Journal of Nuclear Medicine. 2019 Aug 1;60(8):1042-3.

33. F. H. R. France, “Ethics and biomedical information,” International journal of medical informatics, vol. 49, no. 1, pp. 111–115, 1998.
34. Johansson, J., Alakurtti, K., Joutsa, J., Tohka, J., Ruotsalainen, U., & Rinne, J. O. (2016). Comparison of manual and automatic techniques for substriatal segmentation in 11C-raclopride high-resolution PET studies. *Nuclear medicine communications*, *37*(10), 1074–1087. https://doi.org/10.1097/MNM.0000000000000559
35. Dewalle-Vignion, A. S., Yeni, N., Petyt, G., Verscheure, L., Huglo, D., Béron, A., Adib, S., Lion, G., & Vermandel, M. (2012). Evaluation of PET volume segmentation methods: comparisons with expert manual delineations. *Nuclear medicine communications*, *33*(1), 34–42. https://doi.org/10.1097/MNM.0b013e32834d736f
36. Piri, R., Edenbrandt, L., Larsson, M., Enqvist, O., Nøddeskou-Fink, A. H., Gerke, O., & Høilund-Carlsen, P. F. (2022). Aortic wall segmentation in $^{18}$F-sodium fluoride PET/CT scans: Head-to-head comparison of artificial intelligence-based versus manual segmentation. *Journal of nuclear cardiology : official publication of the American Society of Nuclear Cardiology*, *29*(4), 2001–2010. https://doi.org/10.1007/s12350-021-02649-z
37. Danad, I., Raijmakers, P. G., Driessen, R. S., Leipsic, J., Raju, R., Naoum, C., Knuuti, J., Mäki, M., Underwood, R. S., Min, J. K., Elmore, K., Stuijfzand, W. J., van Royen, N., Tulevski, I. I., Somsen, A. G., Huisman, M. C., van Lingen, A. A., Heymans, M. W., van de Ven, P. M., van Kuijk, C., … Knaapen, P. (2017). Comparison of Coronary CT Angiography, SPECT, PET, and Hybrid Imaging for Diagnosis of Ischemic Heart Disease Determined by Fractional Flow Reserve. *JAMA cardiology*, *2*(10), 1100–1107. https://doi.org/10.1001/jamacardio.2017.2471
38. Kajander, S. A., Joutsiniemi, E., Saraste, M., Pietilä, M., Ukkonen, H., Saraste, A., Sipilä, H. T., Teräs, M., Mäki, M., Airaksinen, J., Hartiala, J., & Knuuti, J. (2011). Clinical value of absolute quantification of myocardial perfusion with (15)O-water in coronary artery disease. *Circulation. Cardiovascular imaging*, *4*(6), 678–684. https://doi.org/10.1161/CIRCIMAGING.110.960732
39. Mathur, P., Srivastava, S., Xu, X., & Mehta, J. L. (2020). Artificial Intelligence, Machine Learning, and Cardiovascular Disease. *Clinical Medicine Insights. Cardiology*, *14*, 1179546820927404. https://doi.org/10.1177/1179546820927404

40. WARNER, H. R., TORONTO, A. F., & VEASY, L. G. (1964). EXPERIENCE WITH BAYE'S THEOREM FOR COMPUTER DIAGNOSIS OF CONGENITAL HEART DISEASE. *Annals of the New York Academy of Sciences*, *115*, 558–567.
41. TORONTO, A. F., VEASY, L. G., & WARNER, H. R. (1963). Evaluation of a computer program for diagnosis of congenital heart disease. *Progress in cardiovascular diseases*, *5*, 362–377. https://doi.org/10.1016/s0033-0620(63)80005-5
42. Stenström I, Maaniitty T, Uusitalo V, Pietilä M, Ukkonen H, Kajander S, Mäki M, Bax JJ, Knuuti J, Saraste A. Frequency and angiographic characteristics of coronary microvascular dysfunction in stable angina: a hybrid imaging study. European Heart Journal-Cardiovascular Imaging. 2017 Nov 1;18(11):1206-13.
43. Juarez-Orozco, L. E., Martinez-Manzanera, O., van der Zant, F. M., Knol, R. J. J., & Knuuti, J. (2020). Deep Learning in Quantitative PET Myocardial Perfusion Imaging: A Study on Cardiovascular Event Prediction. *JACC. Cardiovascular imaging*, *13*(1 Pt 1), 180–182. https://doi.org/10.1016/j.jcmg.2019.08.009
44. Zellweger, M. J., Tsirkin, A., Vasilchenko, V., Failer, M., Dressel, A., Kleber, M. E., Ruff, P., & März, W. (2018). A new non-invasive diagnostic tool in coronary artery disease: artificial intelligence as an essential element of predictive, preventive, and personalized medicine. *The EPMA journal*, *9*(3), 235–247. https://doi.org/10.1007/s13167-018-0142-x
45. Zellweger, M. J., Brinkert, M., Bucher, U., Tsirkin, A., Ruff, P., & Pfisterer, M. E. (2014). A new memetic pattern based algorithm to diagnose/exclude coronary artery disease. *International journal of cardiology*, *174*(1), 184–186. https://doi.org/10.1016/j.ijcard.2014.03.184
46. Seifert R, Weber M, Kocakavuk E, Rischpler C, Kersting D. Artificial intelligence and machine learning in nuclear medicine: future perspectives. InSeminars in nuclear medicine 2021 Mar 1 (Vol. 51, No. 2, pp. 170-177). WB Saunders.
47. Dobrucki LW, Sinusas AJ. PET and SPECT in cardiovascular molecular imaging. Nature Reviews Cardiology. 2010 Jan;7(1):38-47.
48. Tarkin JM, Ćorović A, Wall C, Gopalan D, Rudd JH. Positron emission tomography imaging in cardiovascular disease. Heart. 2020 Nov 1;106(22):1712-8.
49. Danad, I., Uusitalo, V., Kero, T., Saraste, A., Raijmakers, P. G., Lammertsma, A. A., Heymans, M. W., Kajander, S. A., Pietilä, M., James, S., Sörensen, J., Knaapen, P., & Knuuti, J. (2014). Quantitative assessment of myocardial perfusion in the detection of significant coronary artery disease: cutoff values and diagnostic accuracy of

quantitative [(15)O]H2O PET imaging. *Journal of the American College of Cardiology*, *64*(14), 1464–1475. https://doi.org/10.1016/j.jacc.2014.05.069

50. Sciagrà, R., Lubberink, M., Hyafil, F., Saraste, A., Slart, R. H. J. A., Agostini, D., Nappi, C., Georgoulias, P., Bucerius, J., Rischpler, C., Verberne, H. J., & Cardiovascular Committee of the European Association of Nuclear Medicine (EANM) (2021). EANM procedural guidelines for PET/CT quantitative myocardial perfusion imaging. *European journal of nuclear medicine and molecular imaging*, *48*(4), 1040–1069. https://doi.org/10.1007/s00259-020-05046-9
51. Nesterov, S. V., Han, C., Mäki, M., Kajander, S., Naum, A. G., Helenius, H., Lisinen, I., Ukkonen, H., Pietilä, M., Joutsiniemi, E., & Knuuti, J. (2009). Myocardial perfusion quantitation with 15O-labelled water PET: high reproducibility of the new cardiac analysis software (Carimas). *European journal of nuclear medicine and molecular imaging*, *36*(10), 1594–1602. https://doi.org/10.1007/s00259-009-1143-8
52. Harjulahti, E., Maaniitty, T., Nammas, W., Stenström, I., Biancari, F., Bax, J. J., Knuuti, J., & Saraste, A. (2021). Global and segmental absolute stress myocardial blood flow in prediction of cardiac events: [15O] water positron emission tomography study. *European journal of nuclear medicine and molecular imaging*, *48*(5), 1434–1444. https://doi.org/10.1007/s00259-020-05093-2
53. Perk, J., De Backer, G., Gohlke, H., Graham, I., Reiner, Z., Verschuren, M., Albus, C., Benlian, P., Boysen, G., Cifkova, R., Deaton, C., Ebrahim, S., Fisher, M., Germano, G., Hobbs, R., Hoes, A., Karadeniz, S., Mezzani, A., Prescott, E., Ryden, L., … ESC Committee for Practice Guidelines (CPG) (2012). European Guidelines on cardiovascular disease prevention in clinical practice (version 2012). The Fifth Joint Task Force of the European Society of Cardiology and Other Societies on Cardiovascular Disease Prevention in Clinical Practice (constituted by representatives of nine societies and by invited experts). *European heart journal*, *33*(13), 1635–1701. https://doi.org/10.1093/eurheartj/ehs092
54. Herzog, B. A., Husmann, L., Valenta, I., Gaemperli, O., Siegrist, P. T., Tay, F. M., Burkhard, N., Wyss, C. A., & Kaufmann, P. A. (2009). Long-term prognostic value of 13N-ammonia myocardial perfusion positron emission tomography added value of coronary flow reserve. *Journal of the American College of Cardiology*, *54*(2), 150–156. https://doi.org/10.1016/j.jacc.2009.02.069
55. Ziadi, M. C., Dekemp, R. A., Williams, K. A., Guo, A., Chow, B. J., Renaud, J. M., Ruddy, T. D., Sarveswaran, N., Tee, R. E., & Beanlands, R. S. (2011). Impaired

myocardial flow reserve on rubidium-82 positron emission tomography imaging predicts adverse outcomes in patients assessed for myocardial ischemia. *Journal of the American College of Cardiology*, *58*(7), 740–748. https://doi.org/10.1016/j.jacc.2011.01.0655

56. R. R. Packard, S.-C. Huang, M. Dahlbom, J. Czernin, and J. Maddahi, "Absolute quantitation of myocardial blood flow in human subjects with or without myocardial ischemia using dynamic flurpiridaz F 18 PET," Journal of Nuclear Medicine, vol. 55, no. 9, pp. 1438–1444, 2014.
57. S. S. Yadav and S. M. Jadhav, "Deep convolutional neural network based medical image classification for disease diagnosis," Journal of Big data, vol. 6, no. 1, pp. 1–18, 2019.
58. Maddahi J, Packard mRR. Cardiac PET perfusion tracers: current status and future directions. InSeminars in nuclear medicine 2014 Sep 1 (Vol. 44, No. 5, pp. 333-343). WB Saunders.
59. Nakazato R, Berman DS, Alexanderson E, Slomka P. Myocardial perfusion imaging with PET. Imaging in medicine. 2013 Feb 1;5(1):35.
60. Kikuchi, Y., Oyama-Manabe, N., Naya, M., Manabe, O., Tomiyama, Y., Sasaki, T., Katoh, C., Kudo, K., Tamaki, N., & Shirato, H. (2014). Quantification of myocardial blood flow using dynamic 320-row multi-detector CT as compared with $^{15}O$-$H_2O$ PET. *European radiology*, *24*(7), 1547–1556. https://doi.org/10.1007/s00330-014-3164-3
61. Pan, L., Cheng, C., Haberkorn, U., & Dimitrakopoulou-Strauss, A. (2017). Machine learning-based kinetic modeling: a robust and reproducible solution for quantitative analysis of dynamic PET data. *Physics in medicine and biology*, *62*(9), 3566–3581. https://doi.org/10.1088/1361-6560/aa6244
62. P. L. da Luz, M. H. Weil, and H. Shubin, "Current concepts on mechanisms and treatment of cardiogenic shock," American Heart Journal, vol. 92, no. 1, pp. 103–113, 1976.
63. D. M. Mancini, T. H. Le Jemtel, S. Factor, and E. H. Sonnenblick, "Central and peripheral components of cardiac failure," The American Journal of Medicine, vol. 80, no. 2, pp. 2–13, 1986.
64. J. A. Kraut and N. E. Madias, "Treatment of acute metabolic acidosis: a pathophysiologic approach," Nature Reviews Nephrology, vol. 8, no. 10, pp. 589–601, 2012.

65. G. D. Giannoglou, Y. S. Chatzizisis, and G. Misirli, “The syndrome of rhabdomyolysis: pathophysiology and diagnosis,” European journal of internal medicine, vol. 18, no. 2, pp. 90100, 2007.
66. T. M. Scarabelli et al., “Clinical implications of apoptosis in ischemic myocardium,” Current problems in cardiology, vol. 31, no. 3, pp. 181–264, 2006.
67. Rainio, O., Han, C., Teuho, J. *et al.* Carimas: An Extensive Medical Imaging Data Processing Tool for Research. *J Digit Imaging* 36, 1885–1893 (2023). https://doi.org/10.1007/s10278-023-00812-1
68. Groot OQ, Bongers MER, Ogink PT, Senders JT, Karhade A v, Bramer JAM, et al. Systematic Review Does Artificial Intelligence Outperform Natural Intelligence in Interpreting Musculoskeletal Radiological Studies? A Systematic Review. Clinical orthopaedics and related research. 2020 Dec;478(12):2751.
69. Brzezicki MA, Bridger NE, Kobetić MD, Ostrowski M, Grabowski W, Gill SS, Neumann S. Artificial intelligence outperforms human students in conducting neurosurgical audits. Clinical Neurology and Neurosurgery. 2020 May 1;192:105732.
70. Doi K. Computer-aided diagnosis in medical imaging: historical review, current status and future potential. Computerized medical imaging and graphics. 2007 Jun 1;31(4-5):198-211.
71. Shiraishi J, Li Q, Appelbaum D, Doi K. Computer-aided diagnosis and artificial intelligence in clinical imaging. InSeminars in nuclear medicine 2011 Nov 1 (Vol. 41, No. 6, pp. 449-462). WB Saunders.
72. Talo M, Baloglu UB, Yıldırım Ö, Acharya UR. Application of deep transfer learning for automated brain abnormality classification using MR images. Cognitive Systems Research. 2019 May 1;54:176-88.
73. Kaur T, Gandhi TK. Deep convolutional neural networks with transfer learning for automated brain image classification. Machine Vision and Applications. 2020 Mar;31(3):1-6.
74. Kim DH, Wit H, Thurston M. Artificial intelligence in the diagnosis of Parkinson’s disease from ioflupane-123 single-photon emission computed tomography dopamine transporter scans using transfer learning. Nuclear medicine communications. 2018 Oct 1;39(10):887-93.
75. LeCun Y, Bengio Y, Hinton G. Deep learning. nature. 2015 May;521(7553):436-44.

76. Choi H. Deep learning in nuclear medicine and molecular imaging: current perspectives and future directions. Nuclear medicine and molecular imaging. 2018 Apr;52(2):109-18.
77. Carbonell JG, Michalski RS, Mitchell TM. An overview of machine learning. Machine learning. 1983 Jan 1:3-23.
78. Simeone O. A very brief introduction to machine learning with applications to communication systems. IEEE Transactions on Cognitive Communications and Networking. 2018 Nov 21;4(4):648-64.
79. Albawi S, Mohammed TA, Al-Zawi S. Understanding of a convolutional neural network. In2017 international conference on engineering and technology (ICET) 2017 Aug 21 (pp. 1-6). Ieee.
80. Gavali P, Banu JS. Deep convolutional neural network for image classification on CUDA platform. InDeep learning and parallel computing environment for bioengineering systems 2019 Jan 1 (pp. 99-122). Academic Press.
81. Sharma N, Jain V, Mishra A. An analysis of convolutional neural networks for image classification. Procedia computer science. 2018 Jan 1;132:377-84.
82. Krizhevsky A, Sutskever I, Hinton GE. Imagenet classification with deep convolutional neural networks. Advances in neural information processing systems. 2012;25.
83. Bigler, M. R., & Seiler, C. (2021). Detection of myocardial ischemia by intracoronary ECG using convolutional neural networks. PloS one, 16(6), e0253200. https://doi.org/10.1371/journal.pone.0253200
84. Genders, T. S., Steyerberg, E. W., Alkadhi, H., Leschka, S., Desbiolles, L., Nieman, K., Galema, T. W., Meijboom, W. B., Mollet, N. R., de Feyter, P. J., Cademartiri, F., Maffei, E., Dewey, M., Zimmermann, E., Laule, M., Pugliese, F., Barbagallo, R., Sinitsyn, V., Bogaert, J., Goetschalckx, K., … CAD Consortium (2011). A clinical prediction rule for the diagnosis of coronary artery disease: validation, updating, and extension. *European heart journal*, *32*(11), 1316–1330. https://doi.org/10.1093/eurheartj/ehr014
85. Juárez-Orozco, L. E., Tio, R. A., Alexanderson, E., Dweck, M., Vliegenthart, R., El Moumni, M., Prakken, N., Gonzalez-Godinez, I., & Slart, R. H. J. A. (2018). Quantitative myocardial perfusion evaluation with positron emission tomography and the risk of cardiovascular events in patients with coronary artery disease: a systematic review of prognostic studies. *European heart journal. Cardiovascular Imaging*, *19*(10), 1179–1187. https://doi.org/10.1093/ehjci/jex331

86. Arsanjani, R., Dey, D., Khachatryan, T., Shalev, A., Hayes, S. W., Fish, M., Nakanishi, R., Germano, G., Berman, D. S., & Slomka, P. (2015). Prediction of revascularization after myocardial perfusion SPECT by machine learning in a large population. *Journal of nuclear cardiology : official publication of the American Society of Nuclear Cardiology*, *22*(5), 877–884. https://doi.org/10.1007/s12350-014-0027-x
87. G. Farias et al., "Automatic feature extraction in large fusion databases by using deep learning approach," Fusion Engineering and Design, vol. 112, pp. 979–983, 2016.
88. A. Gulli and S. Pal, Deep learning with Keras. Packt Publishing Ltd, 2017.
89. P. S. Janardhanan, "Project repositories for machine learning with TensorFlow," Procedia Computer Science, vol. 171, pp. 188–196, 2020.
90. M. M. Najafabadi, F. Villanustre, T. M. Khoshgoftaar, N. Seliya, R. Wald, and E. Muharemagic, "Deep learning applications and challenges in big data analytics," Journal of big data, vol. 2, no. 1, pp. 1–21, 2015.
91. M. Shaha and M. Pawar, "Transfer learning for image classification," in 2018 second international conference on electronics, communication and aerospace technology (ICECA), IEEE, 2018, pp. 656–660.
92. Kriti, J. Virmani, and R. Agarwal, "Deep feature extraction and classification of breast ultrasound images," Multimedia Tools and Applications, vol. 79, pp. 27257–27292, 2020.
93. Prieto-Vargas V, Bautista-P rez-Gavilan A, Lucio-Baez OE, Sierra-Poblete S, Gurrola-Luna H, et al. (2022) PET-Myocardial Perfusion Imaging in the Assessment of Coronary Artery Disease: the basics. Clin Res Trials 8: doi: 10.15761/CRT.1000363.
94. Papandrianos N, Papageorgiou E. Automatic Diagnosis of Coronary Artery Disease in SPECT Myocardial Perfusion Imaging Employing Deep Learning. *Applied Sciences*. 2021; 11(14):6362. https://doi.org/10.3390/app11146362.